

ANNUAL REPORT NASA GRANT NAG-I-629

August 15, 1987

DAMAGE GROWTH IN COMPOSITE
LAMINATES WITH INTERLEAVES

Principal Investigator

James G. Goree

Department of Mechanical Engineering
College of Engineering
Clemson University
Clemson, South Carolina 29634-0921

100-5000
100-5000
NAG-I-629
p. 100

ANNUAL REPORT NASA GRANT NAG-I-629

August 15, 1987

DAMAGE GROWTH IN COMPOSITE
LAMINATES WITH INTERLEAVES

Principal Investigator

James G. Goree
Professor of Mechanics and
Mechanical Engineering
Clemson University
Clemson, South Carolina 29634-0921

Graduate Assistant

Autar K. Kaw
Ph.D. Candidate in
Engineering Mechanics

ABSTRACT

The influence of placing interleaves between fiber reinforced plies in multilayered composite laminates is investigated. The geometry of the composite is idealized as two-dimensional, isotropic, linearly elastic media made of a damaged layer bonded between two half-planes and separated by thin interleaves of low extensional and shear moduli. The damage in the layer is taken in the form of a symmetric crack perpendicular to the interface and may extend up to the interface. The case of an H-shaped crack in the form of a broken layer with delamination along the interface is also analyzed. The interleaves are modeled as distributed shear and tension springs. Fourier integral transform techniques are used to develop solutions in terms of singular integral equations. An asymptotic analysis of the integral equations based on Muskhelishvili's techniques reveals logarithmically singular axial stresses in the half-plane at the crack-tips for the broken layer. For the H-shaped crack, similar singularities are found to exist in the axial stresses at the interface crack-tips in the layer and the half-plane. The solution of the equations is found numerically for the stresses and displacements by using the Hadamard's concept of direct differentiation of Cauchy integrals as well as Gaussian integration techniques.

Numerical results indicate that interleaves increase the interfacial damage tolerance and significantly relieve the stresses in the undamaged plies. Interface cracks (H-shaped cracks) have a stable growth with the mode I opening stress becoming compressive after a small growth. Additional interface crack extension is due to shear stresses

(mode II) only. In order to recommend an interleaf thickness-to-layer width ratio, the influence of relative material properties, structural weight and stress reduction is studied. For example, for a typical Graphite/Epoxy laminate interlayered with thin interleaves made of thermoplastic film, an interleaf thickness of the order of fifteen percent of the layer thickness is recommended.

TABLE OF CONTENTS

	Page
TITLE PAGE	i
ABSTRACT	ii
LIST OF FIGURES	v
LIST OF TABLES	vi
CHAPTER	
I. INTRODUCTION	1
II. FORMULATION AND SOLUTION TECHNIQUES	9
Stress and Displacement Equations	10
Elastic Layer with a Crack	12
Elastic Half-Plane	16
Derivation and Solution of the Integral Equations	17
Crack within the Layer	17
Crack Up to the Interface	28
H-Shaped Crack	42
III. RESULTS AND DISCUSSION	56
Crack within the Layer	57
Crack Up to the Interface	68
H-Shaped Crack	71
Comparison with Experimental Studies	74
IV. CONCLUSIONS	76
APPENDICES	78
A. Integral Expressions and Limit Evaluations	79
B. Definition of Constants	81
C. Stress Intensity Factor for the Embedded Crack	88
D. Cleavage Stress in the Half-Plane for the Broken Layer	90
E. Numerical Techniques and Convergence of Results	93
Crack within the Layer	93
Crack Up to the Interface	94
H-Shaped Crack	97
F. Letter of Consent	102
LIST OF REFERENCES	103

LIST OF FIGURES

Figure	Page
1. Interleafed Prepreg and Cured Laminate Illustrating Retention of Discrete Layer of Tough Resin	2
2. Laminate with a Broken Ply Under Bending and Geometry of the Problem	5
3. Superposition of Two Solutions Used to Solve the Problem of a Stress-Free Crack and Uniform Strain at Infinity	11
4. Classical Half-Plane Problem with Uniform Pressure Over a Finite Range	37
5. Stress Intensity Factor as a Function of Interleaf Thickness for Constant Crack Length (MC I)	59
6. Maximum Cleavage Stress in the Half-Plane as a Function of Interleaf Thickness for Constant Crack Length (MC I)	62
7. Maximum Cleavage Stress in the Half-Plane as a Function of Interleaf Thickness for Constant Crack Length (MC V)	63
8. Transverse Stress Distribution Along the Interface for Constant Crack Length (MC I)	64
9. Maximum Interleaf Transverse Stress as a Function of Interleaf Thickness for Constant Crack Length (MC I)	65
10. Shear Stress Distribution Along the Interface for Constant Crack Length (MC I)	67
11. Maximum Interleaf Shear Stress as a Function of Interleaf Thickness for Constant Crack Length (MC I)	69
12. Modified Stress Intensity Factor as a Function of Interleaf Thickness for Different Material Combinations	70
13. Transverse and Shear Stresses at the Interface Crack-Tip as a Function of Split Length for Constant Interleaf Thickness (MC I)	72
14. Transverse Cracks in Baseline and Interlayered AS4/1808 Laminates at an Impact Energy Level of 800 in-lb/in.	75

LIST OF TABLES

Table	Page
I. Material combinations used	56
II. Maximum interleaf transverse stress for different material combinations ($\frac{a}{h} = 0.9$)	66
III. Maximum interleaf shear stress for different material combinations ($\frac{a}{h} = 0.9$)	66
IV. Length of delamination until closure of crack for different material combinations	73
E-I. Stress intensity factor as a function of number of quadrature points (N)	94
E-II. Modified stress intensity factor as a function of number of collocation points (N)	95
E-III. Estimated values of the normalized modified stress intensity factor	96
E-IV. Modified stress intensity factor as a function of number of collocation points (K, L, M)	101

CHAPTER 1

INTRODUCTION

Laminated fiber reinforced composite materials such as Graphite/Epoxy are being used extensively in aircraft structures and are replacing many metallic components. This is mainly due to their potential for reducing weight and the capacity to be tailored to optimize the structural strength and stiffness. However, due to the fiber and matrix interaction and multi-ply configuration of such composites, the mechanical behavior is quite complex and has challenged the designer with a new class of problems. One particular area which has received considerable attention in the past decade has been their low tolerance to interfacial damage. This type of damage, frequently caused by impact, is a common and an unavoidable occurrence during manufacturing, maintenance and service of aircraft structures.

One suggested method, discussed by Masters [1] and Sun [2], to improve interfacial damage tolerance is to place thin films of adhesive, called interleaves, between those plies where delamination is more likely to occur. This concept is illustrated schematically by Masters [1, Figure 2] and is reproduced here in Figure 1. An interleaf typically has a large shear failure strain and remains a separate layer between plies after curing, unlike the epoxy matrix used in the prepreg plies. Experimental results reported by Masters [1] and Sun [2] do indeed indicate that such adhesive layers are effective in reducing the size of interply delamination, as well as in increasing the load required to initiate delamination. One appropriate view of this problem

ORIGINAL PAGE IS
OF POOR QUALITY

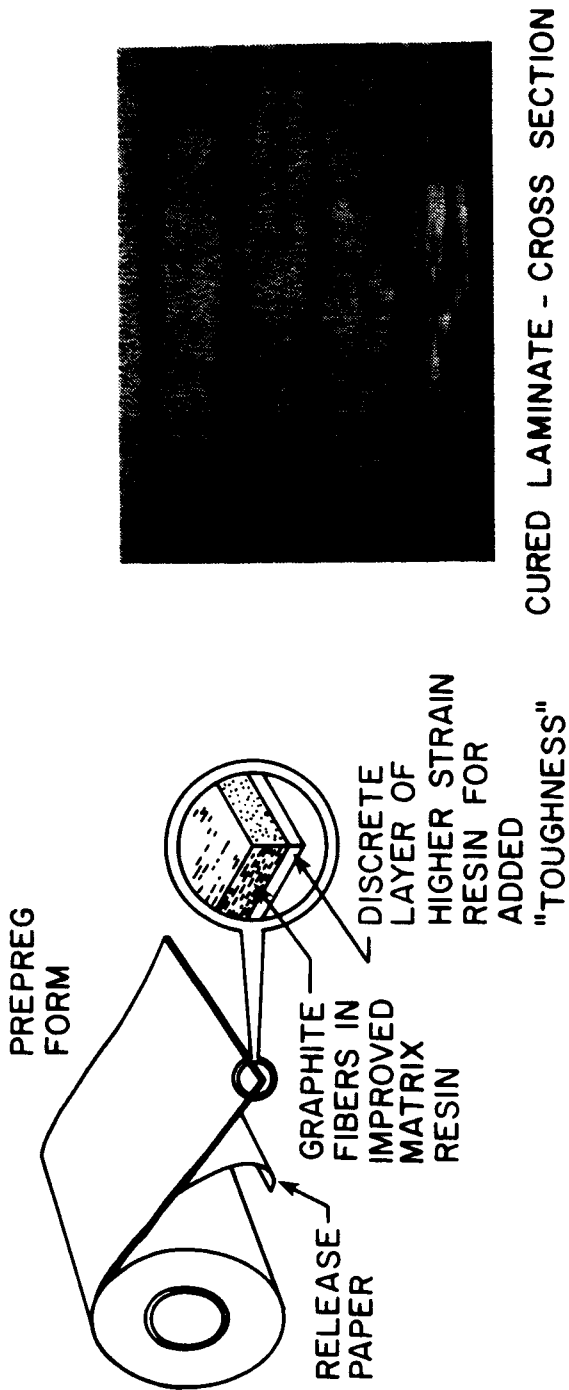


Figure 1. Interleafed Prepreg and Cured Laminate Illustrating Retention of Discrete Layer of Tough Resin (Reproduced from [1] by permission of Mr. John E. Masters, American Cyanamid Company, Stamford, CT 06904).

is that impact typically causes transverse matrix cracks in the 90° plies due to the tensile strains caused by bending. These cracks intersect perpendicular to the 0° plies and may initiate delamination at the ply interfaces. If the ply thickness is small compared to the laminate thickness and the damaged ply is away from the mid-plane on the tensile side, the tensile strain gradient will be small over the ply thickness. The approximation of a uniform tensile strain then should give a good measure of the influence of the crack and the interleaf on delamination. An analytic solution of this problem has, however, not been given adequate treatment. A detailed solution is certainly necessary in order to develop an understanding of the influence of the various material parameters on the behavior of interleaved composites. This is the primary focus of the present study. This problem could be analyzed by using numerical techniques such as finite element methods. But such an approach makes it difficult to conduct parametric studies, find stress singularities, and investigate crack growth behavior, which are important to the designer in determining the strength of the composite and the stress (strain) required for the initiation of damage. The procedure to be followed in the present study is based on a more complete solution of the linear equations of elasticity along with some appropriate simplifying approximations.

A number of related problems have been solved based on various forms of two-dimensional or axisymmetric approximations. Sneddon and Srivastav [3] solved the problem of a transverse crack in a strip of finite width. Gupta and Erdogan [4] considered the problem of two symmetric edge cracks in an infinite strip. Hilton and Sih [5] studied the problem of a strip bonded to two half-planes of different materials with

a crack perpendicular to the interface. Bogy [6] considered the same geometry as in [5] to show analytically the dependence of the solution on material parameters. Both the solutions [5] and [6] allowed only embedded cracks within the strip. Ashbaugh [7] and Gupta [8] reconsidered this problem with the added condition that the crack could propagate up to the interface. Erdogan and Backioglu [9] solved the fracture problem of a composite plate consisting of perfectly bonded parallel load carrying laminates and buffer strips. Gecit and Erdogan [10] relaxed the property of a perfect bond between plies and studied the effect of the thickness and elastic properties of adhesive layers between plies in laminated structures. The problem of two dissimilar elastic bonded half-planes containing a perpendicular crack terminating at the interface was studied by Cook and Erdogan [11]. Goree and Venezia [12] extended this study to include an interface crack that grows along the interface and crosses over the interface. Lu and Erdogan [13] looked at a related problem for the geometry of two dissimilar infinitely long but finite width strips.

The intent of this study is to develop a fracture and crack growth model, and to investigate the influence of an interleaf on damage growth in laminated composites. The composite is approximated by two isotropic half-planes separated from a finite width layer by thin interleaves (Figure 2). This is an idealization of a general laminated composite where one concentrates on a single damaged layer, while the outer layers are approximated by half-planes with average elastic properties. A uniform tensile strain is assumed to be applied to the composite in the y-direction. A typical composite is actually multilayered and orthotropic. The approximation of isotropic, linearly elastic media gives a

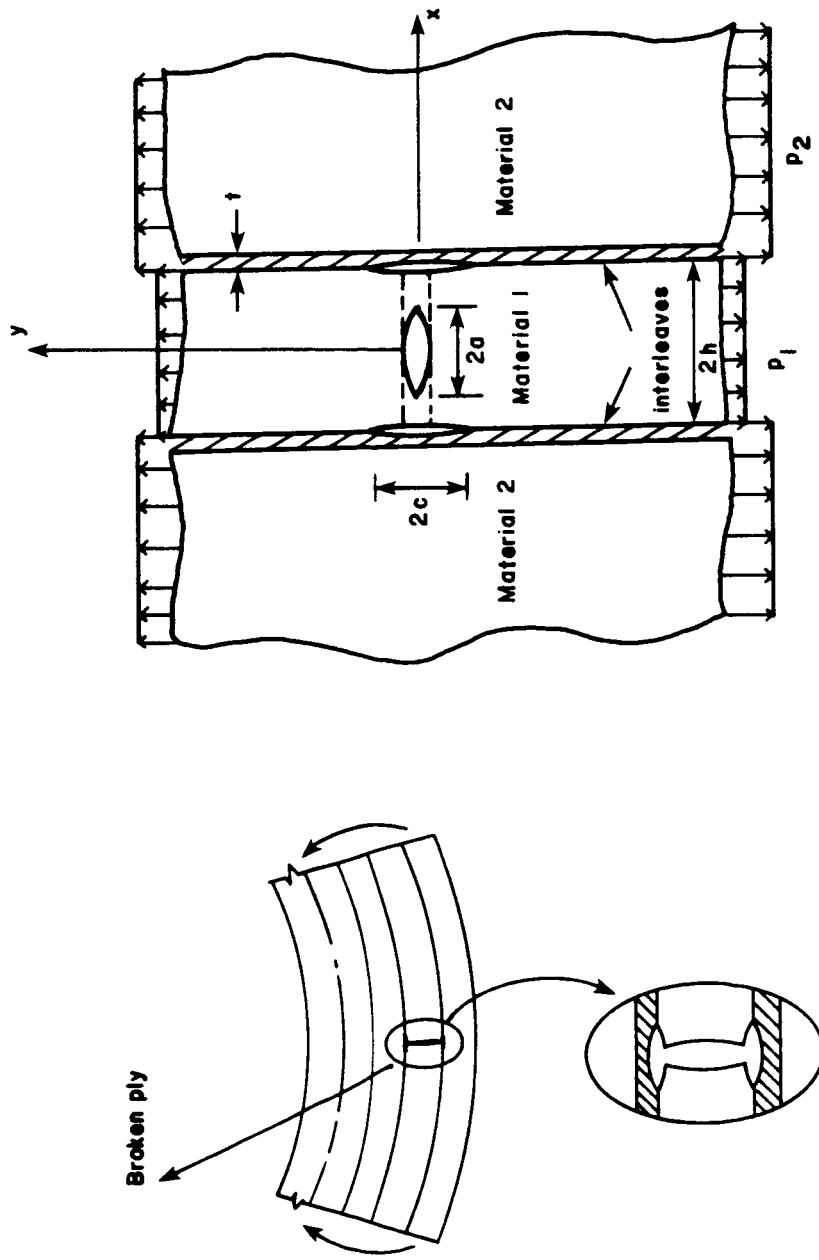


Figure 2. Laminate with a Broken Ply Under Bending and Geometry of the Problem.

more tractable formulation and, along with a proper choice of material constants and thickness ratio, should assist in understanding the influence of the interleaves on damage growth.

The interleaf is modeled as uncoupled distributed tension and shear springs. This is the most sophisticated model, other than an elastic continuum, available in the literature for adhesive layers. Gecit and Erdogan [10] used this spring model to solve the problem of periodically arranged dissimilar layers separated by thin adhesive layers with cracks perpendicular to the interface. However, this approximation was used only for the case of embedded cracks in the layers. For the case of cracks up to the interface of the layers, the spring model was replaced by a continuum model. This made the formulation and the solution cumbersome. For including delamination along the interface, which was not considered in their study, the continuum model for the adhesive layers would involve further complexity in algebraic manipulations and analysis. Other mathematical difficulties involved in including delamination would be the classical singular and oscillatory stresses near an interface crack-tip. The stresses undergo infinite reversals of sign as the crack-tip is approached, and it is also implied that the crack surfaces overlap near the crack-tip which is physically inadmissible. A short literature survey of problems with such oscillatory stresses is given by Cominou in reference [14]. Cominou [14] reconsidered the problem of a traction free interface crack between two dissimilar half-planes in a tension field in an attempt to explain the oscillatory stresses near the crack-tip. She assumed that the crack was not completely open but that the faces were in frictionless contact near the crack-tips. She solved the resulting integral equations for the length of the contact zone and

obtained crack-tip stresses free of oscillatory singularities. Also recently, Gautesen and Dundurs [15] obtained an exact solution for the integral equations developed in [14]. Knowles and Sternberg [16] did not agree with the assumptions of Cominou [14] and solved the problem by using the non-linear theory of elastostatic plane stress. The crack was found to open smoothly near the crack-tips, where the stresses were singular but not of oscillatory type. The spring model, on the other hand, does not involve such controversy and also simplifies the mathematical nature of the model. This simplification is made at the expense of approximating the shear and normal stresses to be constant through the thickness of the interleaf. An interleaf of small thickness and low elastic moduli as compared to those of the plies justifies such an approximation [10]. A detailed discussion of these approximations is presented later in this report. The resulting stresses in the adhesive are finite everywhere, while stresses with logarithmic singularities are shown to occur in the half-planes and the layer at the interface crack-tips.

Based on these approximations, a general formulation is developed for plane strain and generalized plane stress. The displacement and stress fields are expressed in terms of Fourier transforms and, by using Fourier inverse transform techniques, the solution is obtained in closed form in terms of integral equations. These equations are solved by reducing them to simultaneous linear equations using Hadamard's concept of direct differentiation on Cauchy integrals [17] and Gaussian integration techniques [18].

Three cases, depending on the extent of damage, are studied in this work. In the first case the center layer is assumed to have a symmetric

traction-free embedded crack along the x-axis; in the second case the crack touching the interface is analyzed, and lastly damage extending in the form of symmetric delaminations along the interfaces (H-shaped crack) is examined.

The behavior of stresses at critical locations, for example, at the crack-tips, is studied to understand the influence of the relative material properties and geometry of the interleaf and the plies. For the case of a transverse embedded crack, the stresses have a square root singularity. For the cracks touching the interface, the axial stresses in the half-plane at the crack-tip are logarithmically singular. For the H-shaped crack, the axial stresses in the layer and the half-plane at the interface crack-tip are logarithmically singular. The study of these singular stresses and the bounded interleaf stresses are helpful in analyzing the influence of the relative elastic properties and geometry of the interleafed composite on interface debonding, extent and suppression of delamination, and stress relieving in the undamaged plies. The results provide useful information that can assist the designer in the selection of the material and geometrical parameters of the interleaf for a particular baseline laminate.

Certain commercial materials and their manufacturers have been mentioned in this report for a practical discussion of results. The use of these materials in this report is not an official endorsement of these materials or manufacturers, either expressed or implied, by Clemson University.

CHAPTER II
FORMULATION AND SOLUTION TECHNIQUES

Consider a laminated composite (Figure 2) in plane strain or generalized plane stress, consisting of a single layer (Material 1) of width '2h', Young's modulus E_1 and Poisson's ratio ν_1 ; and half-planes (Material 2) having Young's modulus E_2 , and Poisson's ratio ν_2 ; separated by thin interleaves of thickness 't', Young's modulus E_3 and Poisson's ratio ν_3 . This configuration represents a multilayered composite with interleaves where one concentrates on a single layer with damage and approximates the outer undamaged layers by half-planes with averaged elastic properties. The damage considered is a centrally located crack of length '2a' along the x-axis in the layer. This crack may extend up to the interface ($a = h$) to represent a broken layer. A delamination of length '2c' may grow symmetrically along the interface. The geometry is symmetric about the x- and y-axes.

The composite is assumed to be loaded parallel to the y-axis with uniform remote stresses p_1 and p_2 as shown in Figure 2. The remote stresses are related such as to give uniform remote strains in the y-direction. Hence

$$\frac{p_1}{p_2} = \frac{E_1}{E_2} \tag{1.a}$$

for generalized plane stress, and

$$\frac{p_1}{p_2} = \frac{(1-\nu_2^2)E_1}{(1-\nu_1^2)E_2} \tag{1.b}$$

for plane strain.

The solution to the problem of a stress-free crack and loads applied far away from the crack can be obtained by superposing the solutions (Figure 3) of two problems. Let σ_I be the solution to the problem of the composite without cracks and loaded with uniform remote stresses p_1 and p_2 related by equations (1). The solution of this problem is simply a uniform tensile strain throughout the composite. Assume σ_{II} to be the solution to the problem of the composite with damage and having no remote applied loads but with a uniform compression of magnitude p_1 on the transverse crack surface.

The complete solution of the problem is hence given by

$$\sigma_{\text{total}} = \sigma_I + \sigma_{II}. \quad (2)$$

The intent of this study is to find the solution σ_{II} . The solution is found by the use of Fourier transforms and singular integral equation solution techniques [17, 18].

Stress and Displacement Field Equations

The stress and displacement field equation for a cracked layer and a half-plane are developed in this section.

The basic equations for two-dimensional linearly elastic, isotropic medium in the absence of body forces are given in [19]. The governing equilibrium equations are

$$\frac{\partial \sigma_{xx}}{\partial x} + \frac{\partial \sigma_{xy}}{\partial y} = 0, \quad (3.a)$$

$$\frac{\partial \sigma_{xy}}{\partial x} + \frac{\partial \sigma_{yy}}{\partial y} = 0, \quad (3.b)$$

where σ_{xx} , σ_{yy} and σ_{xy} are the components of the stress tensor. The strain-displacement relations are

$$\varepsilon_{xx} = \frac{\partial u}{\partial x}, \quad (4.a)$$

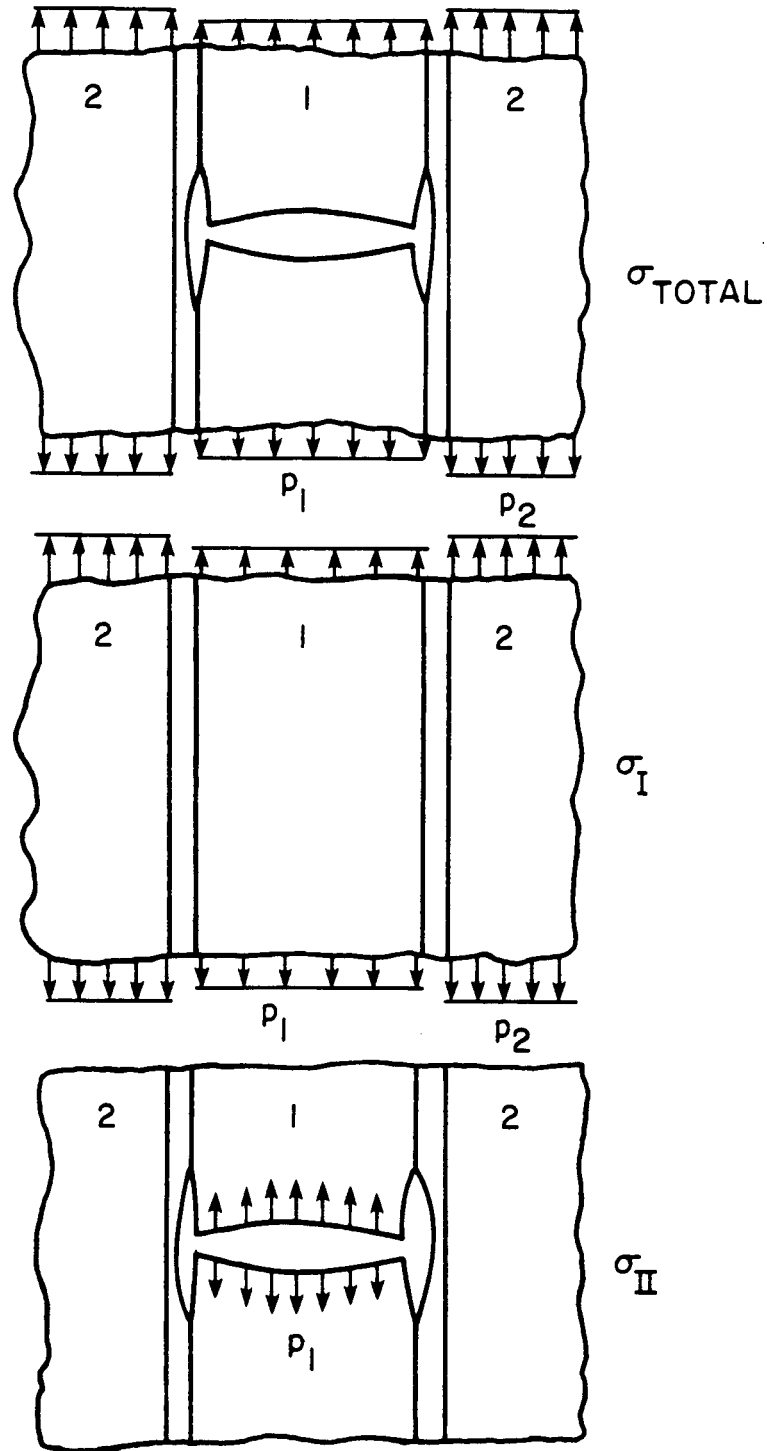


Figure 3. Superposition of Two Solutions Used to Solve the Problem of a Stress-Free Crack and Uniform Strain at Infinity

$$\varepsilon_{yy} = \frac{\partial v}{\partial y}, \quad (4.b)$$

$$\varepsilon_{xy} = \frac{\partial u}{\partial y} + \frac{\partial v}{\partial x}, \quad (4.c)$$

where ε_{xx} , ε_{yy} and ε_{xy} are components of the strain tensor; and u and v are the displacement components in the x - and y -direction, respectively.

The stress-displacement relations are

$$\frac{1}{2\mu} \sigma_{xx} = \frac{\kappa+1}{2(\kappa-1)} \frac{\partial u}{\partial x} + \frac{3-\kappa}{2(\kappa-1)} \frac{\partial v}{\partial y}, \quad (5.a)$$

$$\frac{1}{2\mu} \sigma_{yy} = \frac{3-\kappa}{2(\kappa-1)} \frac{\partial u}{\partial x} + \frac{\kappa+1}{2(\kappa-1)} \frac{\partial v}{\partial y}, \quad (5.b)$$

$$\frac{1}{2\mu} \sigma_{xy} = \frac{1}{2} \left(\frac{\partial u}{\partial y} + \frac{\partial v}{\partial x} \right), \quad (5.c)$$

where μ is the shear modulus, $\kappa = 3-4\nu$ for plane strain, $\kappa = (3-\nu)/(1+\nu)$ for generalized plane stress and ν is Poisson's ratio.

Using the stress-displacement expressions of equations (5), the equilibrium equations (3) can be expressed in terms of displacements as

$$\nabla^2 u + \frac{2}{\kappa-1} \frac{\partial}{\partial x} \left(\frac{\partial u}{\partial x} + \frac{\partial v}{\partial y} \right) = 0, \quad (6.a)$$

$$\frac{2}{\kappa-1} \frac{\partial}{\partial y} \left(\frac{\partial u}{\partial x} + \frac{\partial v}{\partial y} \right) + \nabla^2 v = 0, \quad (6.b)$$

where

$$\nabla^2 = \frac{\partial^2}{\partial x^2} + \frac{\partial^2}{\partial y^2}.$$

Elastic Layer with a Crack

The field equations of a layer with a crack can be obtained by adding the expressions obtained for an uncracked layer (denoted by

superscript 'a') with those of an infinitely large solid with a crack (denoted by superscript 'b').

For an elastic layer without a crack, assume that the displacements are given by the following Fourier transforms,

$$u_1^a(x,y) = \frac{2}{\pi} \int_0^{\infty} F_a(\eta,x) \text{Cos } \eta y \, d\eta, \quad (7.a)$$

$$v_1^a(x,y) = \frac{2}{\pi} \int_0^{\infty} G_a(\eta,x) \text{Sin } \eta y \, d\eta, \quad (7.b)$$

where F_a and G_a are functions determined by the boundary conditions imposed in a particular problem. Substituting equations (7) in equations (6), the mixed differential equations obtained are

$$\frac{\kappa+1}{\kappa-1} \frac{\partial^2 F_a}{\partial x^2} - \eta^2 F_a + \frac{2}{\kappa-1} \eta \frac{\partial G_a}{\partial x} = 0, \quad (8.a)$$

$$-\frac{\partial^2 G_a}{\partial x^2} + \frac{\kappa+1}{\kappa-1} \eta^2 G_a + \frac{2}{\kappa-1} \eta \frac{\partial F_a}{\partial x} = 0. \quad (8.b)$$

Noting that the strip is of finite width and symmetric about the x- and y-axes, the solution of equations (8) is

$$F_a(\eta,x) = -[f_1(\eta) - \frac{\kappa-1}{2} g_1(\eta)] \frac{\text{Sinh } \eta x}{\eta} - g_1(\eta)x \text{Cosh } \eta x, \quad (9.b)$$

$$G_a(\eta,x) = [f_1(\eta) + \frac{\kappa+1}{2} g_1(\eta)] \frac{\text{Cosh } \eta x}{\eta} + g_1(\eta)x \text{Sinh } \eta x, \quad (9.a)$$

where f_1 and g_1 are two unknown functions determined by the boundary conditions of the problem.

For an infinitely large elastic solid with a crack, assume the displacements to be given by the following Fourier transforms,

$$u_1^b(x,y) = \frac{2}{\pi} \int_0^{\infty} F_b(\xi,y) \sin \xi x \, d\xi, \quad (10.a)$$

$$v_1^b(x,y) = \frac{2}{\pi} \int_0^{\infty} G_b(\xi,y) \cos \xi x \, d\xi, \quad (10.b)$$

where F_b and G_b are functions determined by the boundary conditions imposed in a particular problem. Substituting equations (10) in equations (6), the mixed differential equations obtained are

$$\frac{\partial^2 F_b}{\partial y^2} - \frac{\kappa+1}{\kappa-1} \xi^2 F_b - \frac{2}{\kappa-1} \xi \frac{\partial G_b}{\partial y} = 0, \quad (11.a)$$

$$\frac{\kappa+1}{\kappa-1} \frac{\partial^2 G_b}{\partial y^2} - \xi^2 G_b + \frac{2}{\kappa-1} \xi \frac{\partial F_b}{\partial y} = 0. \quad (11.b)$$

Noting that the elastic solid is symmetric about the x- and y-axes and that the stresses and displacements should vanish as $y \rightarrow \infty$, the solution to equations (11) is

$$F_b(\xi,y) = -\frac{\phi_1(\xi)}{\xi} \left(\frac{\kappa-1}{2} - \xi y \right) e^{-\xi y}, \quad (12.a)$$

$$G_b(\xi,y) = \frac{\phi_1(\xi)}{\xi} \left(\frac{\kappa+1}{2} + \xi y \right) e^{-\xi y}, \quad (12.b)$$

where $\phi_1(\xi)$ is an unknown function determined by the boundary conditions.

The displacement field of a cracked layer is now given by

$$u_1(x,y) = u_1^a(x,y) + u_1^b(x,y), \quad (13.a)$$

$$v_1(x,y) = v_1^a(x,y) + v_1^b(x,y). \quad (13.b)$$

Substituting equations (7) and (10) in equations (13) and using equations (9) and (12), the displacement field of a cracked layer is written as

$$\begin{aligned}
u_1(x,y) = & -\frac{2}{\pi} \int_0^{\infty} \left\{ \frac{1}{\eta} \left[f_1(\eta) - \frac{\kappa_1-1}{2} g_1(\eta) \right] \text{Sinh}(\eta x) \right. \\
& \left. + \eta g_1(\eta) \text{Cosh}(\eta x) \right\} \text{Cos}(\eta y) d\eta \\
& - \frac{2}{\pi} \int_0^{\infty} \frac{\phi_1(\xi)}{\xi} \left(\frac{\kappa_1-1}{2} - \xi y \right) e^{-\xi y} \text{Sin}(\xi x) d\xi, \quad (14.a)
\end{aligned}$$

$$\begin{aligned}
v_1(x,y) = & \frac{2}{\pi} \int_0^{\infty} \left\{ \frac{1}{\eta} \left[f_1(\eta) + \frac{\kappa_1+1}{2} g_1(\eta) \right] \text{Cosh}(\eta x) \right. \\
& \left. + \eta g_1(\eta) \text{Sinh}(\eta x) \right\} \text{Sin}(\eta y) d\eta \\
& + \frac{2}{\pi} \int_0^{\infty} \frac{\phi_1(\xi)}{\xi} \left(\frac{\kappa_1+1}{2} + \xi y \right) e^{-\xi y} \text{Cos}(\xi x) d\xi. \quad (14.b)
\end{aligned}$$

Using the strain-displacement relations (4) and the stress-displacement relations (5), the corresponding stress field is given by

$$\begin{aligned}
\frac{\sigma_{xx}^1(x,y)}{2\mu_1} = & -\frac{2}{\pi} \int_0^{\infty} \left[f_1(\eta) \text{Cosh}(\eta x) + \eta x g_1(\eta) \text{Sinh}(\eta x) \right] \text{Cos}(\eta y) d\eta \\
& - \frac{2}{\pi} \int_0^{\infty} \phi_1(\xi) (1-\xi y) e^{-\xi y} \text{Cos}(\xi x) d\xi, \quad (15.a)
\end{aligned}$$

$$\begin{aligned}
\frac{\sigma_{yy}^1(x,y)}{2\mu_1} = & \frac{2}{\pi} \int_0^{\infty} \left\{ \left[f_1(\eta) + 2g_1(\eta) \right] \text{Cosh}(\eta x) \right. \\
& \left. + \eta x g_1(\eta) \text{Sinh}(\eta x) \right\} \text{Cos}(\eta y) d\eta \\
& - \frac{2}{\pi} \int_0^{\infty} \phi_1(\xi) (1+\xi y) e^{-\xi y} \text{Cos}(\xi x) d\xi, \quad (15.b)
\end{aligned}$$

$$\begin{aligned}
\frac{\sigma_{xy}^1(x,y)}{2\mu_1} &= \frac{2}{\pi} \int_0^{\infty} \{ [f_1(\eta) + g_1(\eta)] \text{Sinh}(\eta x) \\
&\quad + \eta x g_1(\eta) \text{Cosh}(\eta x) \} \text{Sin}(\eta y) d\eta \\
&\quad - \frac{2}{\pi} \int_0^{\infty} \xi y \phi_1(\xi) e^{-\xi y} \text{Sin}(\xi x) d\xi.
\end{aligned} \tag{15.c}$$

Elastic Half-Plane

Assuming the same form of displacement given by equations (7), the solution for the elastic half-plane is given by equations (8). Noting the symmetry of the half-plane about the y-axis and that the stresses and displacement should vanish as $x \rightarrow \infty$, the displacement field equations of a half-plane obtained are

$$u_2(x,y) = \frac{2}{\pi} \int_0^{\infty} \left\{ \frac{1}{\eta} [f_2(\eta) + \frac{\kappa_2-1}{2} g_2(\eta)] + x g_2(\eta) \right\} e^{-\eta x} \text{Cos}(\eta y) d\eta, \tag{16.a}$$

$$v_2(x,y) = \frac{2}{\pi} \int_0^{\infty} \left\{ \frac{1}{\eta} [f_2(\eta) - \frac{\kappa_2+1}{2} g_2(\eta)] + x g_2(\eta) \right\} e^{-\eta x} \text{Sin}(\eta y) d\eta. \tag{16.b}$$

By substituting the displacement field equations (16) in the stress-displacement relations (5), the corresponding stress-field equations are given by

$$\frac{\sigma_{xx}^2(x,y)}{2\mu_2} = -\frac{2}{\pi} \int_0^{\infty} [f_2(\eta) + \eta x g_2(\eta)] e^{-\eta x} \text{Cos}(\eta y) d\eta, \tag{17.a}$$

$$\frac{\sigma_{yy}^2(x,y)}{2\mu_2} = \frac{2}{\pi} \int_0^{\infty} [f_2(\eta) + (\eta x - 2) g_2(\eta)] e^{-\eta x} \text{Cos}(\eta y) d\eta, \tag{17.b}$$

$$\frac{\sigma_{xy}^2(x,y)}{2\mu_2} = -\frac{2}{\pi} \int_0^{\infty} [f_2(\eta) + (\eta x - 1)g_2(\eta)] e^{-\eta x} \sin(\eta y) d\eta. \quad (17.c)$$

The unknown functions f_1 , g_1 , ϕ_1 , f_2 and g_2 in the displacement and stress field equations (14-17) are determined by applying appropriate boundary and continuity conditions relating to the problem. The solution is obtained in terms of singular integral equations which can be solved by standard numerical techniques [17, 18].

Derivation and Solution of the Integral Equations

Three cases related to the extent of the damage are investigated. The first case deals with a symmetric transverse crack of length '2a' ($a < h$) located centrally along the x-axis. In the second case, the crack can extend upto the interface ($a = h$) and represents a broken layer. The last case accounts for a crack up to the interface ($a = h$) along with splitting of length '2c' located symmetrically parallel to the y-axis at the interface ($x = \pm h$) (Figure 2) and is more commonly called the H-shaped crack. The nature of the damage effects the continuity and boundary conditions of the problem. Hence, each case is studied separately. The solution is derived in terms of singular integral equations. An asymptotic analysis is carried out to study the singular behavior of stresses and displacement slopes in the vicinity of the crack-tips. Numerical techniques are developed to solve the integral equations for the unknown functions.

Crack within the Layer

As discussed in Chapter 1, the interleaves are modeled as uncoupled distributed tension and shear springs and the stiffness of

these springs is given in [10] as

$$K_n = \frac{E_0}{t}, \quad (18.a)$$

$$K_s = \frac{\mu_3}{t}, \quad (18.b)$$

where

$$E_0 = \frac{E_3}{1-\nu_3^2}$$

for generalized plane stress,

$$= \frac{E_3(1-\nu_3)}{(1+\nu_3)(1-2\nu_3)}$$

for plane strain.

By modeling the interleaf as springs, the transverse and shear stresses are constant through the thickness of the interleaf. The continuity conditions along $x = h$ are then written as

$$\sigma_{xy}^1(h,y) = \sigma_{xy}^2(h,y), \quad 0 \leq |y| < \infty. \quad (19.a)$$

$$\sigma_{xx}^1(h,y) = \sigma_{xx}^2(h,y), \quad 0 \leq |y| < \infty. \quad (19.b)$$

$$\sigma_{xx}^1(h,y) = K_n [u_2(h,y) - u_1(h,y)], \quad 0 \leq |y| < \infty, \quad (20.a)$$

$$\sigma_{xy}^1(h,y) = K_s [v_2(h,y) - v_1(h,y)], \quad 0 \leq |y| < \infty. \quad (20.b)$$

The homogeneous boundary conditions along $y = 0$ are

$$\sigma_{xy}^1(x,0) = 0, \quad |x| < h, \quad (21.a)$$

$$\sigma_{xy}^2(x,0) = 0, \quad |x| > h, \quad (21.b)$$

$$v_2(x,0) = 0, \quad |x| > h. \quad (21.c)$$

The mixed boundary conditions along $y = 0$ are

$$\sigma_{yy}^1(x,0) = -p(x), \quad |x| < a, \quad (22)$$

$$v_1(x,0) = 0, \quad a < |x| < h. \quad (23)$$

The crack surface traction is a constant for this study and is given by $p(x) = p_1$ as defined by the solution σ_{III} in equation (2). However, the problem is formulated here for the general case of crack surface traction as a symmetric function of 'x', where $p(x) = p_1$ is a special case.

Substituting the stress and displacement field equations (14-17) in the continuity conditions (19) and (20), and taking the inverse Fourier transforms in 'y' yields the following simultaneous equations.

$$\begin{aligned} a_{i1} f_1(\eta) + a_{i2}(\eta) g_1(\eta) + a_{i3} f_2(\eta) + a_{i4} g_2(\eta) &= D_i(\eta), \\ (i = 1, \dots, 4), \end{aligned} \quad (24)$$

where a_{ij} , ($i, j = 1, \dots, 4$) and D_i , ($i = 1, \dots, 4$) are given in Appendix B and the integral formulas in Appendix A are used. Equation (24) can be solved simultaneously for f_1 and g_1 in terms of the unknown functions D_i , which are infinite integrals of the function $\phi_1(\xi)$ to obtain

$$f_1(\eta) = \frac{F_1 \alpha_{22} - F_2 \alpha_{12}}{\alpha_{11} \alpha_{22} - \alpha_{21} \alpha_{12}} e^{-\eta h}, \quad (25.a)$$

$$g_1(\eta) = \frac{F_2 \alpha_{11} - F_1 \alpha_{21}}{\alpha_{11} \alpha_{22} - \alpha_{21} \alpha_{12}} e^{-\eta h}, \quad (25.b)$$

where α_{ij} , ($i = 1, 2, j = 1, 2$), and F_i , ($i = 1, 2$) in terms of D_i , ($i = 1, \dots, 4$), are given in Appendix B.

The homogeneous boundary conditions (21) are identically satisfied by the stress and displacement field equations (14-17).

The mixed boundary condition (23) may be expressed as

$$v(x) = v_1(x,0) = \frac{2}{\pi} \int_0^{\infty} \frac{\phi_1(\xi)}{\xi} \left(\frac{\kappa_1 + 1}{2} \right) \text{Cos } \xi x \, d\xi = 0, \quad a < |x| < h. \quad (26)$$

Taking the Fourier cosine transform of equation (26) gives

$$\frac{\phi_1(\xi)}{\xi} = \frac{2}{\kappa_1+1} \int_0^a v(t) \text{Cos} \xi t \, dt. \quad (27)$$

Substituting equation (27) into the expressions for D_i , ($i = 1, \dots, 4$), given in Appendix B, gives

$$(\kappa_1+1)D_i = \int_{-a}^a H_i(\eta, t) v(t) e^{-\eta(h-t)} \, dt, \quad (i = 1, \dots, 4), \quad (28)$$

where $H_i(\eta, t)$, ($i = 1, \dots, 4$), are given in Appendix B. Using these expressions for D_i , the functions F_i , ($i = 1, 2$), used in equation (25) can be expressed as

$$F_i(\eta) = \int_{-a}^a E_i(\eta, t) v(t) e^{-\eta(h-t)} \, dt, \quad (i = 1, 2). \quad (29)$$

The functions E_i , ($i = 1, 2$), are given in Appendix B.

The mixed boundary condition (22) may now be written as

$$\begin{aligned} \frac{\sigma_{yy}^1(x, 0)}{2\mu_1} &= \lim_{y \rightarrow 0^+} -\frac{2}{\pi} \int_0^{\infty} \phi_1(\xi) (1+\xi y) e^{-\xi y} \text{Cos} \xi x \, d\xi \\ &\quad + \frac{2}{\pi} \int_0^{\infty} \{ [f_1(\eta) + 2g_1(\eta)] \text{Cosh} \eta x + \eta x g_1(\eta) \text{Sinh} \eta x \} \, d\eta \\ &= -\frac{p(x)}{2\mu_1}, \quad |x| < a. \end{aligned} \quad (30)$$

With $\phi_1(\xi)$ defined by equation (27), the first integral in equation (30) becomes

$$\begin{aligned} & \lim_{y \rightarrow 0^+} - \frac{2}{\pi} \int_0^{\infty} \phi_1(\xi) (1 + \xi y) e^{-\xi y} \cos \xi x \, d\xi \\ &= \frac{2}{\pi(\kappa_1 + 1)} \int_0^a v(t) \left[\frac{1}{(t-x)^2} + \frac{1}{(t+x)^2} \right] dt. \end{aligned} \quad (31)$$

The even symmetry property of the crack opening displacement, $v(x)$ simplifies the right hand side of equation (31) to

$$\begin{aligned} & \frac{2}{\pi(\kappa_1 + 1)} \int_0^a v(t) \left[\frac{1}{(t-x)^2} + \frac{1}{(t+x)^2} \right] dt \\ &= \frac{2}{\pi(\kappa_1 + 1)} \int_{-a}^a \frac{v(t)}{(t-x)^2} dt. \end{aligned} \quad (32)$$

Substituting equation (29) in equation (25), the unknown functions f_1 and g_1 can be algebraically written as a function of the displacement function $v(x)$. Substituting these results in the second integral of equation (30), and equation (32) in the first integral, a singular integral equation in terms of the unknown displacement function $v(t)$ is obtained as

$$\int_{-a}^a \frac{v(t)}{(t-x)^2} dt + \int_{-a}^a K_{11}(t, x) v(t) dt = - \frac{\pi(1 + \kappa_1)p(x)}{4\mu_1}, \quad |x| < a, \quad (33)$$

where

$$K_{11}(x, t) = \int_0^{\infty} k_{11}(t, x, \eta) e^{-\eta(h-t)} d\eta. \quad (34)$$

The expression for $k_{11}(t, x, \eta)$ is

$$\begin{aligned}
k_{11}(t,x,\eta) = & \{[\alpha_{22}-2\alpha_{21}) \text{Cosh } \eta x - \eta x \alpha_{21} \text{Sinh } \eta x] E_1 \\
& + [(-\alpha_{12}+2\alpha_{11}) \text{Cosh } \eta x + \eta x \alpha_{21} \text{Sinh } \eta x] E_2\} e^{-\eta h} \\
& / (\alpha_{11}\alpha_{22}-\alpha_{21}\alpha_{12}), \tag{35}
\end{aligned}$$

where α_{ij} , ($i = 1,2$, $j = 1,2$), and E_i , ($i = 1,2$), are given in Appendix B.

Using integration by parts, the singular integral equation (33) can be expressed in terms of the slope of the crack opening displacement, defined as

$$G(x) = \frac{\partial v(x)}{\partial x}. \tag{36}$$

The integral equation then has the following form

$$\begin{aligned}
v(a) F(x) + \int_{-a}^a \frac{G(t)}{t-x} dt + \int_{-a}^a G(t) \bar{K}_{11}(t,x) dt = -\frac{\pi p(x)(1+\kappa_1)}{4\mu_1}, \\
|x| < a, \tag{37}
\end{aligned}$$

where

$$\begin{aligned}
F(x) = \int_0^\infty \{ \{ f_{11} [(\alpha_{22}-2\alpha_{21}) \text{Cosh } \eta x - \eta x \alpha_{21} \text{Sinh } \eta x] \\
+ f_{22} [(-\alpha_{12}+2\alpha_{11}) \text{Cosh } \eta x + \eta x \alpha_{11} \text{Sinh } \eta x] \} e^{-\eta h} \\
/ (\alpha_{11}\alpha_{22} - \alpha_{21}\alpha_{12}) - 2 \text{Cosh } \eta x e^{-\eta h} \} d\eta, \tag{38}
\end{aligned}$$

and f_{11} and f_{22} are given in Appendix B.

The integrand $\bar{K}_{11}(t,x)$ is

$$\bar{K}_{11}(t,x) = \int_0^\infty \bar{k}_{11}(t,x,\eta) d\eta, \tag{39}$$

where

$$\begin{aligned} \bar{k}_{11}(t,x,\eta) = & \left\{ [(\alpha_{22}-2\alpha_{21})\text{Cosh } \eta x - \eta x \alpha_{21} \text{ Sinh } \eta x] \frac{\partial E_1}{\partial t} \right. \\ & \left. + [(-\alpha_{12} + 2\alpha_{11}) \text{Cosh } \eta x + \eta x \alpha_{11} \text{ Sinh } \eta x] \frac{\partial E_2}{\partial t} \right\} e^{-\eta h} \\ & / (\alpha_{11}\alpha_{22} - \alpha_{21}\alpha_{12}), \end{aligned} \quad (40)$$

and α_{ij} , ($i = 1,2$, $j = 1,2$), and E_i , ($i = 1,2$) are given in Appendix B.

Since the vertical displacements, $v(\pm a)$ at the crack tips must be identically equal to zero, the integral equation (37) reduces to

$$\int_{-a}^a \frac{G(t)}{t-x} dt + \int_{-a}^a G(t) \bar{K}_{11}(t,x) dt = \frac{-\pi p(x)(1+\kappa_1)}{4\mu_1}, \quad |x| < a. \quad (41)$$

All the special cases can be recovered from equation (41). For example, for the interleaf thickness $t = 0$, equation (41) is identical to that given by equation (17) in [8]. The problem of a layer, with a crack situated perpendicular to the interface, bonded between two half-planes of elastic properties different from the layer was solved by Gupta in [8]. Equation (17) in [8] can also be obtained by making the interleaf infinitely stiff, that is, make the elastic moduli μ_3 and E_3 approach infinity. Note that the interleaf can be made stiffer by either increasing its elastic moduli or by decreasing the interleaf thickness. For the other special case of letting the interleaf thickness approach infinity, equation (41) is identical to equation (19) in [4]. The problem of an infinite strip with an internal crack perpendicular to the stress-free longitudinal edges was solved as a special case by Gupta and Erdogan in [4].

It can be shown that $\bar{k}_{11}(t,x,\eta)$ is a bounded and exponentially decaying function. Hence $\bar{K}_{11}(t,x)$ is also bounded and the singular

integral equation is of the Cauchy-type. The singular behavior of the slope function, $G(t)$ may be analyzed by studying the dominant part of the singular integral equation (41), which can be expressed as

$$\int_{-a}^a \frac{G(t)}{t-x} dt = B(x), \quad |x| < a, \quad (42)$$

where $B(x)$ contains all the bounded terms of equation (41).

Following the technique explained in [8], $G(t)$ is assumed to have an integrable power singularity at $t = \pm a$ which can be written as

$$G(t) = \frac{H(t)}{(a^2-t^2)^\gamma} = \frac{H(t)e^{\pi i \gamma}}{(t-a)^\gamma (t+a)^\gamma}, \quad |t| < a, \quad (43)$$

where $0 < \text{Re} \gamma < 1$ and $H(t)$ satisfies the Holder conditions [20] in the closed interval $[-a, a]$. A function $f(x)$ is said to be Holder continuous in $[-a, a]$, if for any two points x_1, x_2 in $[-a, a]$ $|f(x_2) - f(x_1)| \leq A |x_2 - x_1|^\rho$ is satisfied. A and ρ are positive constants and $0 < \rho < 1$, 'A' is called the Holder constant and ' ρ ' is termed as Holder index.

Consider the sectionally holomorphic function

$$\phi(z) = \frac{1}{\pi} \int_{-a}^a \frac{G(t)}{t-z} dt = \frac{1}{\pi} \int_{-a}^a \frac{H(t)e^{\pi i \gamma}}{(t-a)^\gamma (t+a)^\gamma (t-z)} dt. \quad (44)$$

According to ([20], Chapter 4)

$$\phi(z) = \frac{H(-a)}{(2a)^\gamma} \frac{e^{\pi i \gamma}}{\text{Sin} \pi \gamma} \frac{1}{(z+a)^\gamma} - \frac{H(a)}{(2a)^\gamma} \frac{1}{\text{Sin} \pi \gamma} \frac{1}{(z-a)^\gamma} + \phi_0(z), \quad (45)$$

where $\phi_0(z)$ is bounded everywhere except at the end points $z = \pm a$, where

$$|\phi_0(z)| < \frac{H_0(\pm a)}{|z \pm a|^{\gamma_0}}, \quad \text{Re}(\gamma_0) < \text{Re}(\gamma). \quad (46)$$

Following [8] and using the Plemelj formulas,

$$\phi^+(x) - \phi^-(x) = 2iG(x), \quad |x| < a, \quad (47.a)$$

$$\phi^+(x) + \phi^-(x) = \frac{2}{\pi} \int_{-a}^a \frac{G(t)}{t-x} dt, \quad |x| < a, \quad (47.b)$$

$$\phi(x) = \frac{H(-a) \text{Cot } \pi\gamma}{(2a)^\gamma (a+x)^\gamma} - \frac{H(a) \text{Cot } \pi\gamma}{(2a)^\gamma (a-x)^\gamma} + \phi_0^*(x), \quad |x| < a, \quad (48)$$

where $\phi_0^*(x)$ is a bounded function and has behavior similar to $\phi_0(z)$.

Substituting equation (48) in equation (42) and letting $x \rightarrow a$ or $-a$,

$$\text{Cot } \pi\gamma = 0 \quad (49)$$

is obtained. Equation (49) is called the characteristic equation and in the acceptable range of $0 < \text{Re } \gamma < 1$ has the root

$$\gamma = \frac{1}{2}. \quad (50)$$

Using the above value of γ , equation (43) gives the slope of the displacement as

$$G(t) = \frac{H(t)}{\sqrt{a^2 - t^2}}, \quad |t| < a. \quad (51)$$

Substituting equation (51) in equation (41), the singular integral equation may then be expressed as

$$\int_{-a}^a \frac{H(t)}{\sqrt{a^2 - t^2}} \left[\frac{1}{t-x} + \bar{K}_{1,1}(t,x) \right] dt = -\frac{\pi(1+\kappa_1)p(x)}{4\mu_1}, \quad |x| < a. \quad (52)$$

Since the index of the integral equation (41) is +1 [18], the solution will contain an arbitrary constant, which is determined by the single valuedness condition

$$\int_{-a}^a G(t) dt = 0. \quad (53)$$

Normalizing the variables with respect to the half crack length

'a',

$$s = \frac{t}{a}, \quad (54.a)$$

$$r = \frac{x}{a}, \quad (54.b)$$

$$G(t) = G(as) = \phi(s), \quad (54.c)$$

$$p(x) = p(as) = S(r), \quad (54.d)$$

$$H(t) = H(as) = \Psi(s), \quad (54.e)$$

equation (41) may be written as

$$\int_{-1}^1 \phi(s) \left[\frac{1}{s-r} + a \bar{K}_{11}(as, ar) \right] ds = -\frac{\pi S(r)(1+\kappa_1)}{4\mu_1}, \quad |r| < 1. \quad (55)$$

Using equation (51), the non-dimensional slope function, $\phi(s)$ can be expressed as

$$\phi(s) = \frac{\Psi(s)}{a\sqrt{1-s^2}}, \quad |s| < 1. \quad (56)$$

The integral equation (55) is approximated by using Gauss-Chebyshev integration formulae and techniques [18] to give

$$\begin{aligned} & \frac{1}{N} \sum_{i=1}^N \Psi(s_i) \left[\frac{1}{a(s_i - r_j)} + a \bar{K}_{11}(as_i, ar_j) \right] \\ &= -\frac{\pi S(r_j)(1+\kappa_1)}{4\mu_1}, \quad (j = 1, 2, \dots, N-1), \end{aligned} \quad (57)$$

where

$$s_i = \cos \left[\frac{(2i-1)\pi}{2N} \right], \quad (i = 1, 2, \dots, N), \quad (58)$$

$$r_j = \cos \left[\frac{\pi j}{N} \right], \quad (j = 1, 2, \dots, N-1). \quad (59)$$

Using equation (56), the single valuedness condition (53) can be approximated as

$$\sum_{i=1}^N \Psi(s_i) = 0. \quad (60)$$

Equations (57) and (60) represent a $N \times N$ system of simultaneous linear equations which gives numerical values for $\Psi(s)$ at the discrete points, s_i given by equation (58).

Once $\Psi(s)$ is determined numerically, the unknown functions f_1 , g_1 , f_2 , g_2 , and ϕ_1 can be evaluated using equation (24). This implies that the stresses and displacements can then be obtained at any point.

The normal cleavage stress, $\sigma_{yy}^1(a^+, 0)$ at the crack-tip, has a square root singularity (see Appendix C). A stress intensity factor, K_1 is defined as

$$K_1 = \lim_{x \rightarrow a^+} \sqrt{2(x-a)} \sigma_{yy}^1(x, 0). \quad (61)$$

Equation (55) can be re-written (Appendix C) in non-dimensional terms as

$$K_1 = -\frac{4\mu_1}{(1+\kappa_1)} \frac{\Psi(1)}{\sqrt{a}}. \quad (62)$$

In the numerical solution, the value of the non-dimensional function $\Psi(s)$ can be determined only at discrete points given by equation (58) and the end points (± 1) cannot be chosen as one of these discrete points. Krenk [21] developed a summation formula by using properties of Chebyshev polynomials to give the extrapolated value of $\Psi(1)$ as

$$\Psi(1) = \frac{1}{N} \sum_{i=1}^N \frac{\sin[\frac{2N-1}{4N} (2i-1)\pi]}{\sin[\frac{2i-1}{4N} \pi]} \Psi(s_i). \quad (63)$$

The routines used to solve the kernel $\bar{K}_{11}(x,t)$ and the discussion on the convergence of the results is given in Appendix E. Convergence of the results for similar elastostatic problems obtained by using the techniques discussed for the present case is discussed in detail in [22].

Crack Up to the Interface

The boundary and continuity conditions for the crack extending up to the interface remain the same as for the case of the crack within the layer as discussed in the previous section. Hence, the governing singular integral equation (37) is valid for this case too. However, the Fredholm Kernel $\bar{K}_{11}(t,x)$ becomes unbounded for certain values of x and t . An asymptotic analysis reveals that $\bar{K}_{11}(t,x)$ is unbounded as $x \rightarrow h$ and $t \rightarrow h$ or $x \rightarrow -h$ and $t \rightarrow h$, simultaneously. Since the integrand $\bar{k}_{11}(t,x,\eta)$ in equation (37) is bounded and continuous in the semi-infinite interval $0 < \eta < \infty$, the unbounded terms in $\bar{K}_{11}(x,t)$ are due to the asymptotic behavior of $\bar{k}_{11}(t,x,\eta)$ as $\eta \rightarrow \infty$. The part contributing the unbounded term may be expressed as

$$\bar{K}_{11}^{\infty}(t,x) = \int_0^{\infty} \bar{k}_{11}^{\infty}(t,x,\eta) e^{-\eta(2h-t)} d\eta, \quad (64)$$

with

$$\begin{aligned} \bar{k}_{11}^{\infty}(t,x,\eta) = & [-4h(h-t)\eta^2 + \eta\{6(h-t) + B_1h(h-t) + 2h\} \\ & + \{[B_2h-4+B_3h(h-t) + B_4(h-t)]\} \text{Cosh } \eta x \\ & + [4x(h-t)\eta^2 + \eta\{-B_1x(h-t)-2x\} \\ & + \{-B_2x-B_3x(h-t)\}] \text{Sinh } \eta x, \end{aligned} \quad (65)$$

where the functions B_i , ($i = 1, \dots, 4$), are given in Appendix B.

Using the following integrals [23]

$$\int_0^{\infty} \eta^m e^{-\eta(2h-t)} \text{Sinh } \eta x \, d\eta = \frac{d^m}{dt^m} \left[\frac{x}{(2h-t)^2 - x^2} \right], \quad (66.a)$$

$$\int_0^{\infty} \eta^m e^{-\eta(2h-t)} \text{Cosh } \eta x \, d\eta = \frac{d^m}{dt^m} \left[\frac{2h-t}{(2h-t)^2 - x^2} \right], \quad (66.b)$$

the singular kernel $\bar{K}_{11}^{\infty}(t,x)$ may be written as

$$\begin{aligned} \bar{K}_{11}^{\infty}(t,x) = & \frac{1}{2} \left\{ -4(h-x)^2 \frac{d^2}{dx^2} + [12(h-x) + B_1(h-x)^2] \frac{d}{dx} \right. \\ & \left. + [-2-(B_1+B_2-B_4)(h-x) + B_3(h-x)^2] \right\} \frac{1}{t-(2h-x)} \\ & + \frac{1}{2} \left\{ -4(h+x)^2 \frac{d^2}{dx^2} + [-12(h+x) - B_1(h+x)^2] \right\} \frac{d}{dx} \\ & + [-2-(B_1+B_2-B_4)(h+x) + B_3(h+x)^2] \right\} \frac{1}{t-(2h+x)}. \end{aligned} \quad (67)$$

The coefficient of $v(h)$ in equation (37) also becomes unbounded as $x \rightarrow \pm h$. The asymptotic behavior of $F(x)$ shows that the part contributing the unboundedness may be expressed as

$$F^{\infty}(x) = \int_0^{\infty} f^{\infty}(\eta, x) e^{-\eta h} \, d\eta, \quad (68)$$

where

$$f^{\infty}(\eta, x) = \frac{B_5}{\eta+B_6} \text{Cosh } \eta x, \quad (69)$$

and B_i , ($i = 5,6$), are given in Appendix B.

The behavior of the slope function, $G(t)$ at the end points can now be found by considering the dominant part of the singular integral

equation which can be expressed as

$$v(h) \int_0^{\infty} f^{\infty}(\eta, x) e^{-\eta h} d\eta + \int_{-h}^h G(t) \left[\frac{1}{t-x} + \bar{K}_{11}^{\infty}(t, x) \right] dt = B(x), \quad |x| < h, \quad (70)$$

where $B(x)$ is a bounded function. Assume $G(t)$ to have an integrable singularity at $t = \pm h$ given by

$$G(t) = \frac{H(t)}{(h^2 - t^2)^{\gamma}} = \frac{H(t)e^{\pi i \gamma}}{(t-h)^{\gamma}(t+h)^{\gamma}}, \quad |t| < h, \quad (71)$$

where $0 < \text{Re } \gamma < 1$ and $H(t)$ satisfies the Holder condition in the closed interval $[-h, h]$. Consider the sectionally holomorphic function

$$\phi(z) = \frac{1}{\pi} \int_{-h}^h \frac{G(t)}{t-z} dt. \quad (72)$$

Following the procedure outlined in the previous section and applying the Plemelj formulas (47) to equation (72),

$$\phi(x) = \frac{H(-h)}{(2h)^{\gamma}} \frac{\text{Cot } \pi \gamma}{(h+x)^{\gamma}} - \frac{H(h)}{(2h)^{\gamma}} \frac{\text{Cot } \pi \gamma}{(h-x)^{\gamma}} + \phi_1^*(x), \quad |x| < h, \quad (73.a)$$

$$\phi(2h+x) = -\frac{H(h)}{(2h)^{\gamma}} \frac{1}{\text{Sin } \pi \gamma} \frac{1}{(h+x)^{\gamma}} + \phi_2^*(x), \quad h < 2h + x < 3h, \quad (73.b)$$

$$\phi(2h-x) = -\frac{H(h)}{(2h)^{\gamma}} \frac{1}{\text{Sin } \pi \gamma} \frac{1}{(h-x)^{\gamma}} + \phi_3^*(x), \quad h < 2h - x < 3h, \quad (73.c)$$

where $\phi_i^*(x)$, ($i = 1, 2, 3$), has behavior similar to $\phi_0(z)$ given by equation (46).

Substituting equations (65) and (68) in equation (70) and using equations (69) and (73) to separate the unbounded terms, the following equation is obtained

$$\begin{aligned}
& v(h) [B_5 e^{B_6(h-x)} \log(h-x) + B_5 e^{B_6(h+x)} \log(h+x)] \\
& + \frac{H(h)}{(2h)^\gamma \sin \pi\gamma(h+x)^\gamma} [-\cos \pi\gamma + \frac{1}{2} \{4\gamma(\gamma+1) - 12\gamma + 2\}] \\
& + \frac{H(h)}{(2h)^\gamma \sin \pi\gamma(h-x)^\gamma} [-\cos \pi\gamma + \frac{1}{2} \{4\gamma(\gamma+1) - 12\gamma + 2\}] = \bar{B}(x), \quad (74)
\end{aligned}$$

where $\bar{B}(x)$ is a bounded function.

Multiplying equation (74) by $(h+x)^\gamma$ and substituting $x = -h$ and then multiplying by $(h-x)^\gamma$ and substituting $x = +h$, the resulting characteristic equation is

$$-\cos \pi\gamma + 2\gamma^2 - 4\gamma + 1 = 0. \quad (75)$$

This characteristic equation is independent of material constants and is identical to the characteristic equation obtained for the solution of a free end problem of a strip under self-equilibrating residual stresses [9].

There are no roots of equation (75) in the acceptable range of $0 < \text{Re } \gamma < 1$, which implies that $G(t)$ does not have a power singularity. Hence $G(t)$ either has a logarithmic singularity or is bounded at the end points $t = \pm h$.

If $G(t)$ is a bounded function, then

$$G(t) = H(t), \quad t < |h|, \quad (76)$$

where $H(t)$ satisfies the Holder conditions in the closed interval $[-h, h]$.

Again consider the following sectionally holomorphic function

$$\phi(z) = \int_{-h}^h \frac{G(t)}{t-z} dt = \int_{-h}^h \frac{H(t)}{t-z} dt. \quad (77)$$

According to [20, Chapter 4]

$$\phi(z) = H(h) \log(z-h) - H(-h) \log(z+h) + \phi_0(z), \quad (78)$$

where $\phi_0(z)$ is a bounded function tending to a definite limit when $z \rightarrow \pm h$ along any path. Following [9], using the Plemelj formulas (47), and noting that $G(t)$ is an odd function, the following results are obtained,

$$\phi(x) = H(h) \log(h^2 - x^2) + \phi_1^*(x), \quad |x| < h, \quad (79.a)$$

$$\phi(2h+x) = H(h) \log(h+x) + \phi_2^*(x), \quad h < 2h + x < 3h, \quad (79.b)$$

$$\phi(2h-x) = H(h) \log(h-x) + \phi_3^*(x), \quad h < 2h - x < 3h. \quad (79.c)$$

The functions $\phi_i^*(x)$, ($i = 1, 2, 3$), are bounded functions.

Substituting equation (79) in equation (70) and separating the unbounded terms

$$v(h) [B_5 e^{B_6(h-x)} \log(h-x) + B_5 e^{B_6(h+x)} \log(h+x)] = B(x), \quad (80)$$

where $B(x)$ is a bounded function. The above equality is possible only if the displacement at the end points, $v(\pm h)$ is zero. This is not the case because the interleaf is modeled as distributed tension and shear springs, which allows the broken layer to displace at the end points under a uniform pressure, p_1 on the cracked surface. Hence, $G(t)$ cannot be bounded at the end points. This leaves only the possibility of a logarithmic singularity for $G(t)$ at the end points.

Assume $G(t)$ has an integrable logarithmic singularity at $t = \pm h$ expressed as

$$G(t) = H(t) \log\left(\frac{h+t}{h-t}\right), \quad |t| < h, \quad (81)$$

where $H(t)$ satisfies the Holder condition in the closed interval $[-h, h]$.

Note that since $G(t)$ is an odd function, $H(t)$ must be an even function, that is, $H(t) = H(-t)$.

Consider the sectionally holomorphic functions

$$\begin{aligned}\phi(z) &= \int_{-h}^h \frac{G(t)}{t-z} dt = \int_{-h}^h \frac{H(t) \log\left(\frac{h+t}{h-t}\right)}{t-z} dt \\ &= \phi_1(z) - \phi_2(z),\end{aligned}\tag{82}$$

where

$$\phi_1(z) = \int_{-h}^h \frac{H(t) \log(h+t)}{t-z} dt,\tag{83.a}$$

$$\phi_2(z) = \int_{-h}^h \frac{H(t) \log(h-t)}{t-z} dt,\tag{83.b}$$

According to [20, Chapter 4], near $z = h$,

$$\phi_1(z) = H(h) \log(2h) \log(z-h) + \phi_0(z),\tag{84}$$

where $\phi_0(z)$ is a bounded function tending to a definite limit at $z = h$.

Near $z = -h$,

$$\phi_1(z) = H(h) \int_{-h}^h \frac{\log(h+t)}{t-z} dt + \text{bounded function}.\tag{85}$$

Consider

$$\Omega(z) = \frac{1}{2\pi i} \int_{-h}^h \frac{\log(h+t)}{t-z} dt.\tag{86}$$

Using the Plemelj formulas (47),

$$\Omega^+(t_0) - \Omega^-(t_0) = \log(t_0+h) \quad \text{for } t_0 \in [-h, h].\tag{87}$$

Also

$$\omega^+(t_0) - \omega^-(t_0) = -\log(t_0+h) \quad \text{for } t_0 \in [-h, h], \quad (88)$$

if

$$\omega(z) = \frac{1}{2} \left[\frac{\{\log(z+h)\}^2}{2\pi i} - \log(z+h) \right]. \quad (89)$$

Adding equations (87) and (88),

$$(\Omega+\omega)^+ - (\Omega+\omega)^- = 0, \quad (90)$$

and therefore the function $[\Omega(z) + \omega(z)]$ is holomorphic in the neighborhood of $z = -h$, that is, near $z = -h$,

$$\Omega(z) = -\frac{1}{2} \left[\frac{\{\log(z+h)\}^2}{2\pi i} - \log(z+h) \right] + \text{holomorphic function}. \quad (91)$$

From equations (82), (83), (84) and (91), the behavior of $\phi_1(z)$ near the end points $z = \pm h$ is written as

$$\begin{aligned} \phi_1(z) = H(h) \log(2h) \log(z-h) - \frac{H(h)}{2} [\{\log(z+h)\}^2 - 2\pi i \log(z+h)] \\ + \text{holomorphic function}. \end{aligned} \quad (92)$$

Similarly the behavior of $\phi_2(z)$ near the end points $z = \pm h$ can be expressed as

$$\begin{aligned} \phi_2(z) = H(h) \log(2h) \log(z+h) + \frac{H(h)}{2} [\log(z-h)]^2 \\ + \text{holomorphic function}. \end{aligned} \quad (93)$$

Applying the Plemelj formulas (47) in equations (92) and (93), equation (72) is reduced, for $z = x$, $2h + x$, and $2h - x$, to give

$$\begin{aligned} \phi(x) = H(h) \log(2h) \log(h^2-x^2) - \frac{H(h)}{2} [\{\log(h-x)\}^2 \\ + \{\log(h+x)\}^2] + \phi_1^*(x), \quad |x| < h, \end{aligned} \quad (94.a)$$

$$\begin{aligned} \phi(2h+x) = & -\frac{H(h)}{2} [\log(h+x)]^2 + H(h) \log(2h) \log(h+x) \\ & + \phi_2^*(x), \quad h < 2h + x < 3h, \end{aligned} \quad (94.b)$$

$$\begin{aligned} \phi(2h-x) = & -\frac{H(h)}{2} [\log(h-x)]^2 + H(h) \log(2h) \log(h-x) \\ & + \phi_3^*(x), \quad h < 2h - x < 3h, \end{aligned} \quad (94.c)$$

where $\phi_i^*(x)$, ($i = 1, 2, 3$), are bounded functions.

Substituting equations (94) in equation (70), and separating the unbounded terms

$$\begin{aligned} & [-B_\varepsilon e^{B_\varepsilon(h-x)} \log(h-x) - B_\varepsilon e^{B_\varepsilon(h+x)} \log(h+x)]v(h) \\ & - 4H(h) [\log(h-x) + \log(h+x)] = B(x), \end{aligned} \quad (95)$$

where $B(x)$ contains all the bounded terms. For the boundedness of the left hand side of equation (95), it is required that

$$H(h) = -\frac{B_\varepsilon}{4} v(h) = -\frac{\kappa_1+1}{4\mu_1} \frac{\mu_3}{t} v(h). \quad (96)$$

Noting that

$$\sigma_{xy}^1(h, 0+) = \sigma_{xy}^2(h, 0+) = -\frac{\mu_3}{t} v(h), \quad (97)$$

and

$$H(h) = \frac{\kappa_1+1}{4\mu_1} \sigma_{xy}^1(h, 0+), \quad (98)$$

then

$$\lim_{x \rightarrow \pm h^-} G(x) = \frac{\kappa_1+1}{4\mu_1} \sigma_{xy}^1(h, 0+) \lim_{x \rightarrow \pm h^-} \log\left(\frac{h+x}{h-x}\right). \quad (99)$$

This proves the assumption that the slope, $G(x)$ of the crack opening displacement, $v(x)$ function has a logarithmic singularity at the end

points is correct. Note that the coefficient of the logarithmic term is dependent on the shear stress at the end point, $(x = h, y = 0+)$.

The problem of a crack in the layer extending up to the interface can also be viewed as two semi-infinite strips with uniform pressure, p_1 applied on the transverse axis $(y = 0)$ and unknown finite tractions on the longitudinal sides $(x = \pm h)$. These tractions depend on the elastic properties and geometrical parameters of the interleaf and the half-plane. This geometry can be compared with the known solution for a semi-infinite strip (obtained from the free-body diagram of the classical half-plane problem with uniform pressure over a finite range, Figure 4) having the following boundary conditions

$$\sigma_{xy}(x,0) = 0, \quad -h < x < h, \quad (100.a)$$

$$\sigma_{yy}(x,0) = -p_1, \quad -h \leq x \leq h, \quad (100.b)$$

$$\sigma_{xx}(\pm h,y) = -\frac{p_1}{\pi} \left[\frac{\pi}{2} - \tan^{-1} \frac{y}{2h} - \frac{2hy}{4h^2+y^2} \right], \quad 0 < y < \infty, \quad (100.c)$$

$$\sigma_{xy}(h,y) = -\frac{p_1}{\pi} \frac{4h^2}{4h^2+y^2}, \quad 0 < y < \infty, \quad (100.d)$$

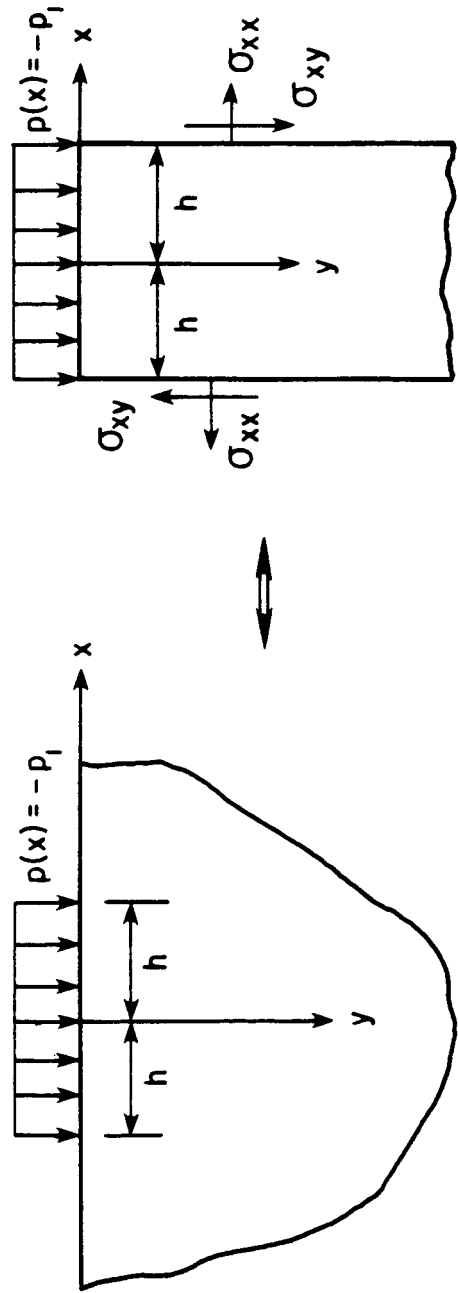
$$\sigma_{xy}(-h,y) = \frac{p_1}{\pi} \frac{4h^2}{4h^2+y^2}, \quad 0 < y < \infty. \quad (100.e)$$

The solution to the above boundary value problem is given in [19, Chapter 5] by using the Airy stress function method. The slope of the vertical displacement is given by

$$\frac{\partial v(x,0)}{\partial x} = -\frac{2p_1}{\pi E} \log\left(\frac{h+x}{h-x}\right), \quad (101.a)$$

or

$$\frac{\partial v(x,0)}{\partial x} = \frac{2}{E} \sigma_{xy}(h,0+) \log\left(\frac{h+x}{h-x}\right). \quad (101.b)$$



$$\sigma_{xy}(h,y) = -\frac{P_1}{\pi} \frac{4h^2}{4h^2+y^2}$$

$$\sigma_{xy}(h,0^+) = -\frac{P_1}{\pi}$$

$$\sigma_{xx}(h,y) = -\frac{P_1}{\pi} \left[\frac{\pi}{2} - \tan^{-1} \frac{y}{2h} - \frac{2hy}{4h^2+y^2} \right]$$

Figure 4. Classical Half-Plane Problem with Uniform Pressure Over a Finite Range

It is interesting to note that both the problems have a logarithmic singularity at the end points $x = \pm h$. In fact, equations (99) and (101.b) are identical expressions for the slope function, $G(x)$ at $x = \pm h$. A finite non-zero shear stress at the point ($x = \pm h, y = 0+$) is the reason for the logarithmically singular slope functions in the two problems.

The shear stress in the half-plane is discontinuous, non-zero and finite at $x = h, y = 0$. Hence, the axial normal stress is logarithmically singular [19, 24] at $x = h, y = 0$ in the half-plane and is given by

$$\lim_{x \rightarrow h^+} \sigma_{yy}^2(x, 0) = \tilde{K} \lim_{x \rightarrow h^+} \log(x-h) + \text{Order}(1), \quad (102)$$

where \tilde{K} is a modified stress intensity factor given by

$$\tilde{K} = \frac{4}{\pi} \sigma_{xy}^1(h, 0+) = -\frac{4\mu_3 v(h)}{\pi t}. \quad (103)$$

The same expression is obtained by an asymptotic analysis (see Appendix D). It is interesting to note that a discontinuity in the normal loads on the half-plane does not produce unbounded stresses.

The numerical techniques enumerated in [18] to solve singular integral equations with Cauchy kernels are based on the exact Cauchy principal value integral expression [25] of orthogonal Jacobi polynomials, $P_n(t)$ given by

$$\int_{-1}^1 \frac{(1-t)^\alpha (1+t)^\beta P_n^{(\alpha, \beta)}(t)}{t-x} dt$$

$$= \pi \cot(\alpha\pi) (1-x)^\alpha (1+x)^\alpha P_n^{(\alpha, \beta)}(x) - \frac{2^{\alpha+\beta} \Gamma(\alpha) \Gamma(n+\beta+1)}{\Gamma(n+\alpha+\beta+1)}$$

$$F(n+1; -n-\alpha-\beta; 1-\alpha; \frac{1-x}{2}) (\alpha > -1, \beta > -1, \alpha \neq 0, 1, 2, \dots), |x| < 1, \quad (104)$$

where $\Gamma(\alpha)$ is the Gamma function and $F(\alpha;\beta;\gamma;z)$ is a hypergeometric series. This relationship forms the basis for solving singular integral equations with a simple Cauchy kernel, where the unknown slope function has a power singularity of the order of (α) and (β) at the end points. But in the present case the slope function has a logarithmic singularity at the end points for which a similar numerical technique could not be found in the literature. Hence solving equation (33) for the unknown displacement function, $v(x)$ is suggested.

Normalizing the following variables with respect to the half-layer width 'h',

$$s = \frac{t}{h}, \quad (105.a)$$

$$r = \frac{x}{h}, \quad (105.b)$$

$$V(s) = h v(t), \quad (105.c)$$

$$K_{11}(r,s) = h^2 K_{11}(t,x), \quad (105.d)$$

$$S(r) = p(x), \quad (105.e)$$

equation (33) can be re-written in the non-dimensional form as

$$\int_{-1}^1 \frac{V(s)}{(s-r)^2} ds + \int_{-1}^1 h^2 V(s) K_{11}(hs,hr) ds = -\frac{\pi S(r)(1+\kappa_1)}{4\mu_1}, \quad |r| < 1. \quad (106)$$

Equation (106) has $\frac{1}{(s-r)^2}$ type integrands and are called strong singularities. Such integrands are classically non-integrable and cannot be defined even in the principal value sense. A concept used by

Hadamard [17] interprets improper integrals of such singularities in the finite part sense. Kaya and Erdogan [26] used this concept to solve elastodynamic problems such as the problem of an edge crack perpendicular to the free boundary of an elastic half-plane.

Using the Cauchy principal value integrals [27]

$$\int_{-1}^1 \frac{P_n(t)}{t-x} dt = -2 Q_n(x), \quad |x| < 1, \quad (107)$$

where $P_n(t)$ and $Q_n(x)$ are Legendre polynomials of the first and the second kind, respectively.

The Hadamard's concept uses direct differentiation on Cauchy integrals to obtain finite part integrals. This is given by

$$\frac{d}{dx} \int_{-1}^1 \frac{f(t)}{t-x} dt = \int_{-1}^1 \frac{f(t)}{(t-x)^2} dt. \quad (108)$$

Using the above direct differentiation in equation (107),

$$\int_{-1}^1 \frac{P_n(t)}{(t-x)^2} dt = -\frac{2(n+1)}{(1-x^2)} [x Q_n(x) - Q_{n-1}(x)], \quad |x| < 1, \quad (109)$$

and assuming

$$V(s) = \sum_{n=0}^N A_n P_n(s), \quad (110)$$

equation (106) can be written as

$$\begin{aligned} \sum_{n=0}^N A_n \left[\frac{-2(n+1)}{1-r^2} \{r Q_n(r) - Q_{n+1}(r)\} + \int_{-1}^1 h^2 P_n(s) K_{11}(hs, hr) ds \right] \\ = \frac{\pi S(r)(1+\kappa_1)}{4\mu_1}, \quad |r| < 1. \end{aligned} \quad (111)$$

A collocation method is used to solve for unknown coefficients, A_n . The choice of collocation points, symmetrically distributed on the interval $(-1,1)$, is not restricted but more points concentrated near the end points improves the rate of convergence. The roots of the Legendre polynomials are a suitable choice of collocation points to give

$$\sum_{n=0}^N A_n \left[\frac{-2(n+1)}{1-r_i^2} \{r_i Q_n(r_i) - Q_{n+1}(r_i)\} + \int_{-1}^1 h^2 P_n(s) K_{1,1}(hs, hr_i) ds \right] = \frac{\pi S(r_i)(1+\kappa_1)}{4\mu_1}, \quad (i = 0, 1, 2, \dots, N-1, N), \quad (112)$$

where r_i is the i^{th} zero of the Legendre polynomial $P_{N+1}(x)$, and

$$P_N(x) = \frac{1}{2^N N!} \frac{d^N}{dx^N} [x^2-1]^N. \quad (113)$$

Equation (112) represents a $[(N+1) \times (N+1)]$ system of linear equations which can be used to numerically evaluate the coefficients, A_n . Using equation (110) the crack opening displacement can be determined. Stresses and displacements can be evaluated by finding functions f_1 , g_1 , f_2 , g_2 and ϕ_1 via equation (24).

The modified stress intensity factor, \tilde{K} defined by equation (103) is expressed numerically as

$$\tilde{K} = -\frac{4\mu_3 h}{\pi t} \sum_{n=0}^N A_n. \quad (114)$$

The routines used to evaluate the kernel $K_{1,1}$ and the finite integral over $[-1,1]$ in Equation (111), as well as the convergence of the results are discussed in Appendix E.

H-Shaped Crack

The damage considered in this case is a broken layer ($a = h$) with delamination of length ' $2c$ ' along the interface (Figure 2). By including delamination, only the continuity conditions along $x = h$ are different from the previous two sections, and these are given by

$$\sigma_{xx}^1(h,y) = \sigma_{xx}^2(h,y), \quad 0 < |y| < \infty, \quad (115.a)$$

$$\sigma_{xy}^1(h,y) = \sigma_{xy}^2(h,y), \quad 0 \leq |y| < \infty, \quad (115.b)$$

$$\begin{aligned} \sigma_{xx}^1(h,y) &= 0, & 0 \leq |y| < c, \\ &= K_n[u_2(h,y) - u_1(h,y)], & c < |y| < \infty. \end{aligned} \quad (116)$$

$$\begin{aligned} \sigma_{xy}^1(h,y) &= 0, & 0 \leq |y| < c, \\ &= K_s[v_2(h,y) - v_1(h,y)], & c < |y| < \infty. \end{aligned} \quad (117)$$

Defining two unknown functions, $\phi_2(y)$ and $\phi_3(y)$ by

$$\frac{2\mu_1\phi_2(y)}{\kappa_1+1} = \sigma_{xx}^1(h,y) - K_n[u_2(h,y) - u_1(h,y)], \quad 0 \leq |y| < \infty, \quad (118)$$

$$-\frac{2\mu_1\phi_3(y)}{\kappa_1+1} = \sigma_{xy}^1(h,y) - K_s[v_2(h,y) - v_1(h,y)], \quad 0 \leq |y| < \infty, \quad (119)$$

the continuity conditions (116) and (117) can be re-written as

$$\sigma_{xx}^1(h,y) = 0, \quad 0 \leq |y| < c, \quad (120)$$

$$\frac{2\mu_1\phi_2(y)}{\kappa_1+1} = \sigma_{xx}^1(h,y) - K_n[u_2(h,y) - u_1(h,y)], \quad |y| < c, \quad (121)$$

$$\phi_2(y) = 0, \quad |y| > c, \quad (122)$$

$$\sigma_{xy}^1(h,y) = 0, \quad 0 \leq |y| < c, \quad (123)$$

$$-\frac{2\mu_1\phi_3(y)}{\kappa_1+1} = \sigma_{xy}^1(h,y) - K_S[v_2(h,y) - v_1(h,y)], \quad |y| < c, \quad (124)$$

$$\phi_3(y) = 0, \quad |y| > c. \quad (125)$$

Substituting the stress and displacement equations (14-17) in equations (115), (120), (121), (123) and (124) and taking the inverse Fourier transforms of the resulting equations in 'y', and using the integral formulas given in Appendix A, the following equations are obtained.

$$a_{i1}f_1(\eta) + a_{i2}g_1(\eta) + a_{i3}f_2(\eta) + a_{i4}g_2(\eta) = L_i(\eta),$$

$$(i = 1, \dots, 4), \quad (126)$$

where a_{ij} , ($i = 1, \dots, 4$, $j = 1, \dots, 4$), and L_i , ($i = 1, \dots, 4$), are given in Appendix B.

Using the mixed boundary condition

$$\frac{\phi_1(\xi)}{\xi} = \frac{2}{\kappa_1+1} \int_0^a v(t) \text{Cos}\xi t \, dt. \quad (27)$$

for $a = h$, and the continuity conditions

$$\phi_2(y) = 0, \quad |y| > c, \quad (122)$$

$$\phi_3(y) = 0, \quad |y| > c, \quad (125)$$

the right hand side, L_i , ($i = 1, \dots, 4$), of equation (126) is expressed as finite integrals in terms of the unknown functions $v(t)$, $\phi_2(y)$ and $\phi_3(y)$ and are given in Appendix B.

Equation (126) can be solved simultaneously for f_1 and g_1 in terms of the three unknown functions $v(t)$, $\phi_2(y)$ and $\phi_3(y)$ to obtain

$$f_1(\eta) = \frac{M_1\alpha_{22} - M_2\alpha_{12}}{\alpha_{11}\alpha_{22} - \alpha_{21}\alpha_{12}} e^{-\eta h},$$

$$g_1(\eta) = \frac{M_2\alpha_{11} - M_1\alpha_{21}}{\alpha_{11}\alpha_{22} - \alpha_{21}\alpha_{12}} e^{-\eta h}, \quad (127)$$

where α_{ij} , ($i = 1, 2, j = 1, 2$), are given in Appendix B, and

$$\begin{aligned}
 M_1(\eta) &= \frac{1}{\kappa_1+1} \left[\int_{-h}^h E_1 e^{-\eta(h-t)} v(t) dt - \lambda_3 \eta \int_0^c \phi_2(y) \cos \eta y dy \right. \\
 &\quad \left. - \lambda_4 \eta \int_0^c \phi_3(y) \sin \eta y dy \right], \\
 M_2(\eta) &= \frac{1}{\kappa_1+1} \left[\int_{-h}^h E_2 e^{-\eta(h-t)} v(t) dt + \lambda_5 \eta \int_0^c \phi_2(y) \cos \eta y dy \right. \\
 &\quad \left. - \lambda_6 \eta \int_0^c \phi_3(y) \sin \eta y dy \right]. \tag{128}
 \end{aligned}$$

where E_i , ($i = 1, 2$) are given in Appendix B.

The homogeneous boundary conditions given by equations (21) are identically satisfied by the stress and displacement field equations (14-17).

Following the same procedure given in the first section of this chapter the mixed boundary condition (22) can be written in the form of a singular integral equation given by

$$\begin{aligned}
 &\int_{-h}^h \frac{v(t)}{(t-x)^2} dt + \int_{-h}^h K_{11}(x,t)v(t) dt + \int_0^c K_{12}(x,z) \phi_2(z) dz \\
 &+ \int_0^c K_{13}(x,z) \phi_3(z) dz = - \frac{\pi p(x)(1+\kappa_1)}{4\mu_1}, \quad |x| < h, \tag{129}
 \end{aligned}$$

where

$$K_{11}(x,t) = \int_0^{\infty} k_{11}(x,t,\eta) e^{-\eta(h-t)} d\eta, \tag{130.a}$$

$$K_{12}(x,z) = \int_0^{\infty} k_{12}(x,\eta) \cos \eta z \, d\eta, \quad (130.b)$$

$$K_{13}(x,z) = \int_0^{\infty} k_{13}(x,\eta) \sin \eta z \, d\eta, \quad (130.c)$$

and

$$\begin{aligned} k_{11}(x,t,\eta) = & \{[(\alpha_{22}-2\alpha_{21}) \cosh \eta x - \eta x \alpha_{21} \sinh \eta x] E_1 \\ & + [(-\alpha_{12}+2\alpha_{11}) \cosh \eta x + \eta x \alpha_{11} \sinh \eta x] E_2\} e^{-\eta h} \\ & /(\alpha_{11}\alpha_{22}-\alpha_{12}\alpha_{21}), \end{aligned} \quad (131.a)$$

$$\begin{aligned} k_{12}(x,\eta) = & \{ -[(\alpha_{22}-2\alpha_{21}) \cosh \eta x - \eta x \alpha_{21} \sinh \eta x] \lambda_3 \\ & + [(-\alpha_{12}+2\alpha_{11}) \cosh \eta x + \eta x \alpha_{11} \sinh \eta x] \lambda_5 \} \eta e^{-\eta h} \\ & /(\alpha_{11}\alpha_{22}-\alpha_{12}\alpha_{21}), \end{aligned} \quad (131.b)$$

$$\begin{aligned} k_{13}(x,\eta) = & \{ -[(\alpha_{22}-2\alpha_{21}) \cosh \eta x - \eta x \alpha_{21} \sinh \eta x] \lambda_4 \\ & - [(-\alpha_{12}+2\alpha_{11}) \cosh \eta x + \eta x \alpha_{11} \sinh \eta x] \lambda_6 \} \eta e^{-\eta h} \\ & /(\alpha_{11}\alpha_{22}-\alpha_{12}\alpha_{21}), \end{aligned} \quad (131.c)$$

where α_{ij} , ($i = 1,2$, $j = 1,2$), and E_i , ($i = 1,2$), are given in Appendix B.

Similarly, by substituting equations (126) and (127) in equation (120) and separating the dominant part of the kernels, the following integral equation is obtained.

$$\begin{aligned} & \int_{-h}^h K_{21}(y,t)v(t)dt + \int_0^c K_{22}(y,z) \phi_2(z)dz - \frac{\pi}{2} \phi_2(y) \\ & + \int_0^c K_{23}(y,z) \phi_3(z)dz = 0, \quad 0 \leq y < c, \end{aligned} \quad (132)$$

where

$$K_{21}(y,t) = \int_0^{\infty} k_{21}(t,\eta) e^{-\eta(h-t)} \text{Cos } \eta y \, d\eta, \quad (133.a)$$

$$K_{22}(y,z) = \int_0^{\infty} [k_{22}(\eta) + 1] \text{Cos } \eta y \text{Cos } \eta z \, d\eta, \quad (133.b)$$

$$K_{23}(y,z) = \int_0^{\infty} k_{23}(\eta) \text{Cos } \eta y \text{Sin } \eta z \, d\eta, \quad (133.c)$$

and

$$\begin{aligned} k_{21}(t,\eta) = & \{ [\alpha_{22} \text{Cosh } \eta h - \eta \alpha_{21} \text{Sinh } \eta h] E_1 \\ & + [-\alpha_{12} \text{Cosh } \eta h + \eta \alpha_{11} \text{Sinh } \eta h] E_2 \} e^{-\eta h} \\ & / (\alpha_{11} \alpha_{22} - \alpha_{12} \alpha_{21}), \end{aligned} \quad (134.a)$$

$$\begin{aligned} k_{22}(\eta) = & \{ -[\alpha_{22} \text{Cosh } \eta h - \eta \alpha_{21} \text{Sinh } \eta h] \lambda_3 \\ & + [-\alpha_{12} \text{Cosh } \eta h + \eta \alpha_{11} \text{Sinh } \eta h] \lambda_5 \} \eta e^{-\eta h} \\ & / (\alpha_{11} \alpha_{22} - \alpha_{12} \alpha_{21}), \end{aligned} \quad (134.b)$$

$$\begin{aligned} k_{23}(\eta) = & \{ -[\alpha_{22} \text{Cosh } \eta h - \eta \alpha_{21} \text{Sinh } \eta h] \lambda_4 \\ & - [-\alpha_{12} \text{Cosh } \eta h + \eta \alpha_{11} \text{Sinh } \eta h] \lambda_6 \} \eta e^{-\eta h} \\ & / (\alpha_{11} \alpha_{22} - \alpha_{12} \alpha_{21}). \end{aligned} \quad (134.c)$$

Similarly by substituting equations (126) and (127) in equation (123) and after separating the dominant part of the kernel, the following integral equation is obtained.

$$\begin{aligned} & \int_{-h}^h K_{31}(y,t) v(t) dt + \int_0^c K_{32}(y,z) \phi_2(z) dz + \int_0^c K_{33}(y,z) \phi_3(z) dz \\ & - \frac{\pi}{2} \phi_3(y) = 0, \quad 0 \leq y < c, \end{aligned} \quad (135)$$

where

$$K_{31}(y,t) = \int_0^{\infty} k_{31}(t,\eta) e^{-\eta(h-t)} \text{Sin } \eta y \, d\eta, \quad (136.a)$$

$$K_{32}(y,z) = \int_0^{\infty} k_{32}(\eta) \text{Cos } \eta z \text{Sin } \eta y \, d\eta, \quad (136.b)$$

$$K_{33}(y,z) = \int_0^{\infty} [k_{33}(\eta) + 1] \text{Sin } \eta z \text{Sin } \eta y \, d\eta, \quad (136.c)$$

$$k_{31}(y,t,\eta) = \left\{ [(\alpha_{22}-\alpha_{21}) \text{Sinh } \eta h - \alpha_{21} \eta h \text{Cosh } \eta h] E_1 + [-\alpha_{12}+\alpha_{11}) \text{Sinh } \eta h + \alpha_{11} \eta h \text{Cosh } \eta h] E_2 \right\} e^{-\eta h} / (\alpha_{11}\alpha_{22}-\alpha_{12}\alpha_{21}), \quad (137.a)$$

$$k_{32}(\eta) = \left\{ -[(\alpha_{22}-\alpha_{21}) \text{Sinh } \eta h - \alpha_{21} \eta h \text{Cosh } \eta h] \lambda_3 + [(-\alpha_{12}+\alpha_{11}) \text{Sinh } \eta h + \alpha_{11} \eta h \text{Cosh } \eta h] \lambda_5 \right\} \eta e^{-\eta h} / (\alpha_{11}\alpha_{22}-\alpha_{12}\alpha_{21}), \quad (137.b)$$

$$k_{33}(\eta) = \left\{ -[(\alpha_{22}-\alpha_{21}) \text{Sinh } \eta h - \alpha_{21} \eta h \text{Cosh } \eta h] \lambda_4 - [(-\alpha_{12}+\alpha_{11}) \text{Sinh } \eta h + \alpha_{11} \eta h \text{Cosh } \eta h] \lambda_6 \right\} \eta e^{-\eta h} / (\alpha_{11}\alpha_{22}-\alpha_{12}\alpha_{21}), \quad (137.c)$$

and the functions α_{ij} , ($i = 1,2$, $j = 1,2$), and E_i , ($i = 1,2$), are given in Appendix B.

Using integration by parts, the singular integral equation (129) can be obtained in terms of the slope of the crack opening displacement integral function

$$G(x) = \frac{\partial v(x)}{\partial x}, \quad (36)$$

such that

$$\begin{aligned}
v(h) F(x) + \int_{-h}^h \frac{G(t)}{t-x} dt + \int_{-h}^h G(t) \bar{K}_{11}(t,x) dt + \int_0^c K_{12}(x,z) \phi_2(z) dz \\
+ \int_0^c K_{13}(x,z) \phi_3(z) dz = -\frac{\pi p(x)(1+\kappa_1)}{4\mu_1}, \quad |x| < h, \quad (138)
\end{aligned}$$

Assume $G(t)$ is a bounded function, then

$$G(t) = H(t), \quad (139)$$

where $H(t)$ satisfies the Holder conditions in the closed interval $[-h, h]$.

For $c = 0$, equation (138) reduces to equation (33) obtained for the case of the crack up to the interface. Hence the first three terms in equation (138) contribute the unbounded terms given by the left hand side of equation (80) expressed as

$$U_1(x) = v(h) [B_5 e^{B_5(h-x)} \log(h-x) + B_5 e^{B_5(h+x)} \log(h+x)]. \quad (140)$$

The unbounded terms contributed by the fifth term of the singular integral equation (138) are given by

$$\bar{U}_2(x) = \int_0^c K_{13}^{\infty}(x,z) \phi_3(z) dz, \quad (141)$$

where

$$K_{13}^{\infty}(x,z) = \int_0^{\infty} k_{13}^{\infty}(x,\eta) \sin \eta z d\eta, \quad (142)$$

and $k_{13}^{\infty}(x,\eta)$ is the asymptotic value of $k_{13}(x,\eta)$ as $\eta \rightarrow \infty$ and is given by

$$k_{13}^{\infty}(x,\eta) = [\eta(h-x) + N_1] e^{-\eta(h-x)} + [-\eta(h+x) + N_2] e^{-\eta(h+x)}, \quad (143)$$

where N_i , ($i = 1, 2$), are given in Appendix B. Using the following results [23]

$$\int_0^{\infty} \eta^m e^{-\eta(h-x)} \sin \eta z \, d\eta = \frac{d^m}{dx^m} \left[\frac{z}{(h-x)^2 + z^2} \right], \quad (144)$$

$$\begin{aligned} K_{1,3}^{\infty}(x,z) &= (h-x) \frac{2(h-x)z}{[(h-x)^2 + z^2]^2} + N_1 \frac{z}{[(h-x)^2 + z^2]} \\ &\quad - (h+x) \frac{2(h+x)z}{[(h+x)^2 + z^2]^2} + N_2 \frac{z}{[(h+x)^2 + z^2]}. \end{aligned} \quad (145)$$

Note that $K_{1,3}^{\infty}(x,z)$ becomes unbounded only as $x \rightarrow \pm h$ and $z \rightarrow 0$ simultaneously.

Consider the following integral

$$\begin{aligned} I &= \int_0^c \frac{z \phi_3(z)}{(h+x)^2 + z^2} \, dz \\ &= \frac{1}{2} \left[\int_0^c \frac{\phi_3(z)}{z+i(h+x)} \, dz + \int_0^c \frac{\phi_3(z)}{z-i(h+x)} \, dz \right]. \end{aligned} \quad (146)$$

According to [20, Chapter 4] near $x = -h$,

$$I = -\phi_3(0) \log(h+x) + \text{bounded function}. \quad (147)$$

Similarly

$$\int_0^c \frac{z \phi_3(z)}{(h-x)^2 + z^2} \, dz = -\phi_3(0) \log(h-x) + \text{bounded function}. \quad (148)$$

From equations (145), (147) and (148), the unbounded part contributed by the fifth term in the integral equation (122) is

$$U_2(x) = -\phi_3(0) \log(h-x) - \phi_3(0) \log(h+x). \quad (149)$$

Following the same procedure, the fourth term in equation (138) is found to have no unbounded terms.

Adding equations (140) and (149), and using equations (123) and (124),

$$U_1(x) + U_2(x) = 0, \quad (150)$$

from which it follows that the sum total of the unbounded terms cancels out. This then proves that the assumption of a bounded slope function, $G(t)$ is correct.

Similar behavior of the slope function was reported by Erdogan and Backioglu [9] for the problem of a semi-infinite strip of finite width '2h' under a self-equilibrating pressure on the transverse end ($y = 0$) and stress-free ends ($x = \pm h$).

The axial stress in the half-plane has a logarithmic singularity at $x = h$, $y = c$. This is the well known logarithmic singularity [19, 24] due to the finite discontinuity in the shear load on a half-plane and is given by

$$\lim_{x \rightarrow h^+} \sigma_{yy}^2(x, c) = K \lim_{x \rightarrow h^+} \log(x-h) + \text{Order}(1), \quad (151)$$

where K is the modified stress intensity factor and is defined by

$$\begin{aligned} K &= \frac{2}{\pi} \sigma_{xy}^1(h, c+) = \frac{2}{\pi} \frac{\mu_3}{t} [v_2(h, c) - v_1(h, c)] \\ &= \frac{4\mu_1}{\pi(\kappa_1 + 1)} \phi_3(c-). \end{aligned} \quad (152)$$

The expression (151) can also be derived by an asymptotic analysis similar to that given in Appendix C. The axial stress in the half-plane at $x = h$, $y = 0$ is bounded, as the shear load is continuous and zero at that point.

The axial stress in the layer is also logarithmically singular at the interface crack-tip ($x = h$, $y = c$), and is given by

$$\lim_{x \rightarrow h^-} \sigma^1_{yy}(x, c) = - K \lim_{x \rightarrow h^-} \log(h-x) + \text{Order}(1). \quad (153)$$

Note that for a split length approaching zero, the modified SIF, K , is exactly half the value of the modified SIF, \tilde{K} given by equation (103) for the case of the broken layer ($a = h$). This is because the discontinuity in the shear load on the half-plane reduces by one-half for an infinitesimal split length.

Normalizing the dimensions of equations (129), (132) and (135) with respect to the half-layer width 'h' and the half split length 'c',

$$s = \frac{t}{h}, \quad (154.a)$$

$$r = \frac{x}{h}, \quad (154.b)$$

$$w = \frac{z}{c}, \quad (154.c)$$

$$q = \frac{y}{c}, \quad (154.d)$$

$$v(t) = \theta_1(s)h, \quad (154.e)$$

$$\phi_2(z) = \theta_2(w)c, \quad (154.f)$$

$$\phi_3(z) = \theta_3(w)c, \quad (154.g)$$

$$p(x) = S(r), \quad (154.h)$$

the following integral equations are obtained in a non-dimensional form.

$$\int_{-1}^1 \frac{\theta_1(s)}{(s-r)^2} ds + \int_{-1}^1 h^2 K_{11}(hr, hs) \theta_1(s) ds + \int_0^1 c^2 K_{12}(hr, cw) \theta_2(w) dw$$

$$+ \int_0^1 c^2 K_{13}(hr, cw) \theta_3(w) dw = - \frac{\pi S(r)(1+\kappa_1)}{4\mu_1}, \quad |r| < 1, \quad (155)$$

$$\int_{-1}^1 h^2 K_{21}(cq, hs) \theta_1(s) ds + \int_0^1 c^2 K_{22}(cq, cw) \theta_2(w) dw - \frac{\pi c}{2} \theta_2(q)$$

$$+ \int_0^1 c^2 K_{23}(cq, cw) \theta_3(w) dw = 0, \quad 0 < q < 1, \quad (156)$$

$$\int_{-1}^1 h^2 K_{31}(cq, hs) \theta_1(s) ds + \int_0^1 c^2 K_{23}(cq, cw) \theta_2(w) dw$$

$$+ \int_0^1 c^2 K_{33}(cq, cw) \theta_3(w) dw - \frac{\pi c}{2} \theta_3(q) = 0, \quad 0 < q < 1. \quad (157)$$

To find the numerical solution to the three integral equations (155-157), the following form of the unknown functions is assumed

$$\theta_1(s) \approx \sum_{k=0}^K A_k P_k(s), \quad (158.a)$$

$$\theta_2(w) \approx \sum_{\ell=0}^L B_\ell T_\ell(w), \quad (158.b)$$

$$\theta_3(w) \approx \bar{C}_0 + \sum_{m=1}^M C_m T_m(w), \quad (158.c)$$

where $P_k(s)$ and $T_\ell(w)$ are Legendre and Chebyshev polynomials of the

first kind, respectively. The normalized crack-opening displacement function $\theta_1(s)$ is approximated by a series of Legendre polynomials because of the availability of a direct relationship (109) for integrands with strong singularities. The other normalized displacement functions $\theta_2(w)$ and $\theta_3(w)$ are approximated by a series of Chebyshev polynomials. It has been shown [28] that a series of Chebyshev polynomials converges more rapidly than any other series of Gegenbauer polynomials, and converges much more rapidly than power series.

Using the Hadamard concept, expressed mathematically by equation (103) for Legendre polynomials, the series approximations (158) for the unknown functions $\theta_i(s)$, ($i = 1, 2, 3$), and the even and odd symmetry of $\theta_2(w)$ and $\theta_3(w)$, respectively, equations (155-157) can be re-written as

$$\sum_{k=0}^K A_k Z_{11}(k, r) + \sum_{\ell=0}^L B_{\ell} Z_{12}(\ell, r) + \sum_{m=0}^M C_m Z_{13}(m, r) = \frac{\pi S(r)(1+\kappa_1)}{4\mu_1}, \quad |r| < 1, \quad (159)$$

$$\sum_{k=0}^K A_k Z_{21}(k, q) + \sum_{\ell=0}^L B_{\ell} Z_{22}(\ell, q) + \sum_{m=0}^M C_m Z_{23}(m, q) = 0, \quad |q| < 1, \quad (160)$$

$$\sum_{k=0}^K A_k Z_{31}(k, q) + \sum_{\ell=0}^L B_{\ell} Z_{32}(\ell, q) + \sum_{m=0}^M C_m Z_{33}(m, q) = 0, \quad |q| < 1, \quad (161)$$

where Z_{ij} , ($i = 1, 2, 3$, $j = 1, 2, 3$) are given in Appendix B.

Note that since the displacement function $\theta_3(w)$ is an odd function of 'w' and is non-zero at $w = 0$, the first term of the series

approximation of the function $\theta_3(w)$ is assumed to be of the form

$$\bar{C}_0 = C_0 \text{ sign } (w),$$

where

$$\begin{aligned} \text{sign } (w) &= +1, \quad \text{if } w > 0, \\ &= -1, \quad \text{if } w < 0. \end{aligned}$$

The collocation method is used to solve for the unknowns A_k , B_ℓ and C_m . The choice of collocation points is distributed symmetrically on the interval $(-1,1)$ for equations (159-161). More points are concentrated near the end points to improve the rate of convergence. The roots of the Legendre polynomials satisfy such a selection of collocation points. Assuming r_{k1} , $q_{\ell 1}$ and p_{m1} as the k th, ℓ th and m th zero of the Legendre polynomials, $P_{K+1}(s)$, $P_{L+1}(w)$ and $P_{M+1}(w)$, respectively, equations (159-161) can be re-written as

$$\begin{aligned} &\sum_{k=0}^K A_k Z_{11}(k, r_{k1}) + \sum_{\ell=0}^L B_\ell Z_{12}(\ell, r_{k1}) + \sum_{m=0}^M C_m Z_{13}(m, r_{k1}) \\ &= \frac{\pi S(r_{k1})(1+\kappa_1)}{4\mu_1}, \quad (k1 = 0, 1, \dots, K-1, K), \end{aligned} \quad (162)$$

$$\begin{aligned} &\sum_{k=0}^K A_k Z_{21}(k, q_{\ell 1}) + \sum_{\ell=0}^L B_\ell Z_{22}(\ell, q_{\ell 1}) + \sum_{m=0}^M C_m Z_{23}(m, q_{\ell 1}) = 0, \\ &(\ell 1 = 0, 1, \dots, L-1, L), \end{aligned} \quad (163)$$

$$\begin{aligned} &\sum_{k=0}^K A_k Z_{31}(k, q_{m1}) + \sum_{\ell=0}^L B_\ell Z_{32}(\ell, q_{m1}) + \sum_{m=0}^M C_m Z_{33}(m, q_{m1}) = 0, \\ &(m1 = 0, 1, \dots, M-1, M). \end{aligned} \quad (164)$$

Equations (162-164) represent a $[(K+L+M+3) \times (K+L+M+3)]$ system of linear equations which can be simultaneously solved for the unknown coefficients A_k , B_l , C_m . The unknown function θ_i , ($i=1,2,3$), can hence be calculated by using equations (158). Stresses and displacements can be evaluated at any point by using equation (126).

The modified stress intensity factor given by equation (152) can be numerically expressed as

$$K = \frac{\Lambda}{\pi(\kappa_1+1)} \sum_{m=0}^M C_m \quad (165)$$

The numerical scheme to evaluate the kernels K_{ij} , ($i = 1,2,3$, $j = 1,2,3$), and the finite integrals in equations (162-164) is explained in Appendix E. Convergence of results is also discussed.

CHAPTER III

RESULTS AND DISCUSSION

The results presented here are for the case of plane strain with a constant pressure, p_1 , on the crack surface and no loads at infinity. This is the solution denoted by σ_{II} in equation (2). The complete solution, σ_{total} can be obtained simply by adding the uniform strain solution, σ_I , which is given by constant stresses as

$$\sigma_{yy}^1 = p_1, \tag{166.a}$$

$$\sigma_{yy}^2 = p_1 \frac{(1-\nu_1^2)E_2}{(1-\nu_2^2)E_1}. \tag{166.b}$$

Five material combinations, given in Table I, are used in the results and are abbreviated as MC I, MC II, etc. for convenience.

Table I. Material combinations used.

Material Combinations	Layer		Half-Plane		Interleaf	
	E_1 (MPA)	ν_1	E_2 (MPA)	ν_2	E_3 (MPA)	ν_3
MC I	10.35	.28	182.90	.28	3.45	.35
MC II	31.05	.28	10.35	.28	3.45	.35
MC III	10.35	.28	10.35	.28	3.45	.35
MC IV	182.90	.28	182.90	.28	3.45	.35
MC V	182.90	.28	10.35	.28	3.45	.35

The Young's moduli E_1 and E_2 in the material combination MC I are the properties in the 90° and 0° directions of a unidirectional T300/5208 Graphite/Epoxy laminate. MC I is the most significant material combination because a transverse notch is more likely to develop first in a 90° ply. This behavior was observed by Masters [1] in his experimental study of impact loading of laminates. Most of the sample results shall hence be discussed for this material combination. The interleaf properties² were supplied by Masters as used in his experimental study [1].

Crack within the Layer

In this problem, a symmetric transverse crack of length ' $2a$ ' ($a/h < 1$)³ is situated in the layer and is opened by a uniform pressure, p_1 . The crack-tip axial stress has a square root type singularity and the coefficient of this singularity is defined as the mode I stress intensity factor (SIF), K_I given by equation (61). When the SIF reaches a critical value $K_I = K_{Ic}$, the crack will propagate. This critical value is called the fracture toughness and is assumed to be constant for a particular material. It should be pointed out that the SIF depends on the crack length and the applied load. This criterion can be directly used only for brittle materials and needs modification for ductile

-
1. T300/5208 Graphite/Epoxy composite laminate is made of T300-graphite fibers (manufactured by Union Carbide) in Rigidite 5208-epoxy resin (registered trademark of Narmco Materials).
 2. Private communication of Professor J. G. Goree, Mechanical Engineering Department, Clemson University, Clemson, SC 29634 with Mr. John E. Masters, Chemical Research Division, American Cyanamid Company, Stamford, CT 06904.
 3. a/h = Crack length to layer width ratio.

materials, where yielding may exist. The simplicity of the criterion, however, makes it a single parameter to predict crack growth and fracture, and is useful even for cracks where yielding is in the form of small plastic zones.

Before presenting the detailed results, the adequacy of modeling the interleaves as distributed shear and tension springs will be discussed. Gecit and Erdogan [10] solved the problem of embedded cracks in periodic buffer strips separated by adhesive layers and modeled the latter both as springs and as a continuum. They found small differences in the results obtained for the two models if the interleaf moduli and thickness were smaller than the strips. For example, for a material combination close to MC III and MC IV, and $a/h = 0.9$ and $(t/h < 0.2)^4$, a difference of less than 3% was found in the SIFs. Results from the present study for the normalized stress intensity factor, $\frac{K_1}{p_1 \sqrt{a}}$ are plotted as a function of interleaf thickness in Figure 5 for MC I. The values of the normalized SIF corresponding to the special cases of an interleaf thickness of zero as well as that of the thickness approaching infinity are found to be in excellent agreement with those special cases found in the literature. For the interleaf thickness approaching infinity, which is equivalent to an interleaf moduli of zero, or therefore corresponding to stress-free longitudinal sides of the layer, the normalized SIFs reach asymptotic values identical to those obtained by Sneddon and Srivastav [3]. They solved the problem of a transverse crack in a finite width strip with unloaded longitudinal edges. The normalized SIF for the other special case of an interleaf thickness of being exactly

4. t/h = Interleaf thickness to half-layer width ratio.

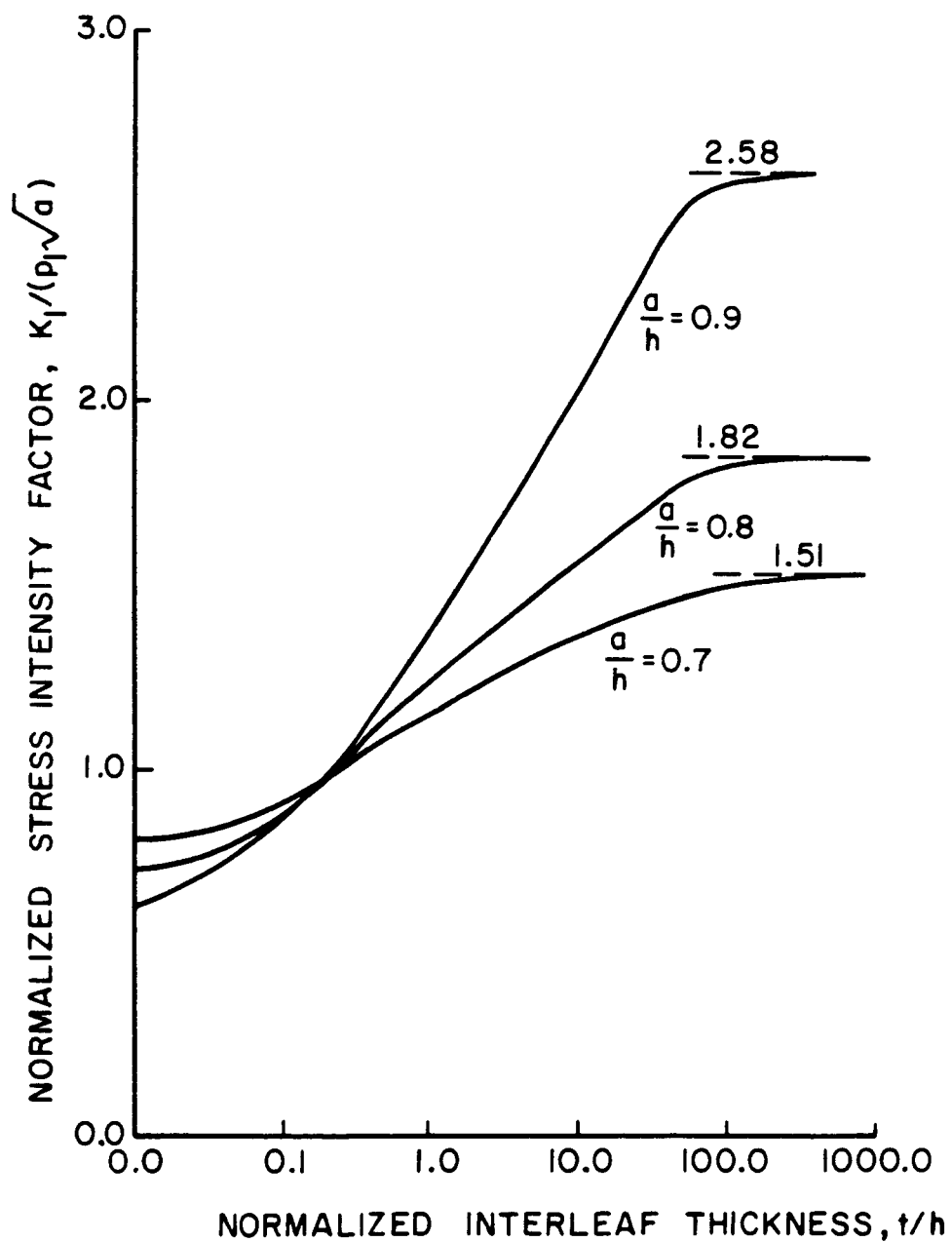


Figure 5. Stress Intensity Factor as a Function of Interleaf Thickness for Constant Crack Length (MC I)

equal to zero are found to be identical to those obtained by Hilton and Sih [5] and Bogy [6]. They solved the problem of a layer, with an internal crack normal to the interface, bonded between two half-planes. These limit cases and the results of Gecit and Erdogan [10] for thin interleaves give considerable assurance as to the usefulness of the results in predicting the behavior of the interleaved composite laminates with an embedded crack.

Additional significant results may be obtained from Figure 5, where it is seen that the normalized SIF increases with an increase in the interleaf thickness. This behavior is true for all material combinations. It does not, however, imply that the global strength of the laminate is necessarily decreased by interleaving laminates. For example, if initial damage is in a 90° ply, the presence of the interleaf may result in a complete failure of the ply at a lower load. The subsequent behavior of the laminate when this ply is fully broken, and the influence of the interleaf on delamination, additional ply failure, and ultimate laminate strength may be higher than with no interleaf. This behavior is considered in the next two sections.

Further, from Figure 5, the SIF (numerator of the normalized SIF) is found to decrease as the crack length is increased for small interleaf thicknesses. Since the SIF is directly related to the load carrying capacity of a material, a decreasing SIF implies a higher load required to continue the crack. The crack growth is hence considered to be stable. For example, for $a/h = 0.9$ and $t/h < 0.08$, the crack growth is stable. This behavior of a stable crack for small interleaf thicknesses holds only for MC I, that is, for the case of the crack in a layer which is weaker than the half-plane.

The maximum cleavage stress, $\frac{\sigma_{yy}^2(h,0)}{p_1}$ in the half-plane occurs in line with the crack-tip at the interface and is plotted in Figure 6 as a function of interleaf thickness for MC I. For small crack lengths ($a/h < 0.8$) this stress is an increasing function in the range of small interleaf thicknesses (or large interleaf moduli) but is relieved on further increase in the thickness. This behavior is not found for large crack lengths. For example, for $a/h = 0.9$, the stress decreases monotonically with an increase in the interleaf thickness. Interestingly, for material combination MC V, where the crack is in a stiffer material, the increase in the cleavage stress in the range of small interleaf thicknesses is much more substantial for all crack lengths as shown in Figure 7. In such cases the introduction of a thin interleaf can, in fact, cause higher cleavage stresses and perhaps assist in continuing the crack across the interface.

Figure 8 shows the transverse stress distribution along the interface for MC I. The stress is maximum and is tensile at $y = 0$, and decreases rapidly to become compressive away from the crack. Figure 9 shows that the maximum transverse stress (at $y = 0$) decreases as the interleaf thickness is increased for MC I. This behavior is found to be typical and is exhibited for all material combinations. Table II gives the maximum interleaf transverse stress for different material combinations for a particular value of $a/h = 0.9$. The percentage decrease due to the introduction of the interleaf is given in parentheses.

Figure 10 shows the shear stress distribution along the interface. This stress is identically equal to zero at $y = 0$ and is very small near $y = 0$, but it changes sign and reaches a maximum value at about half a crack length away from the crack. The maximum interleaf shear stress,

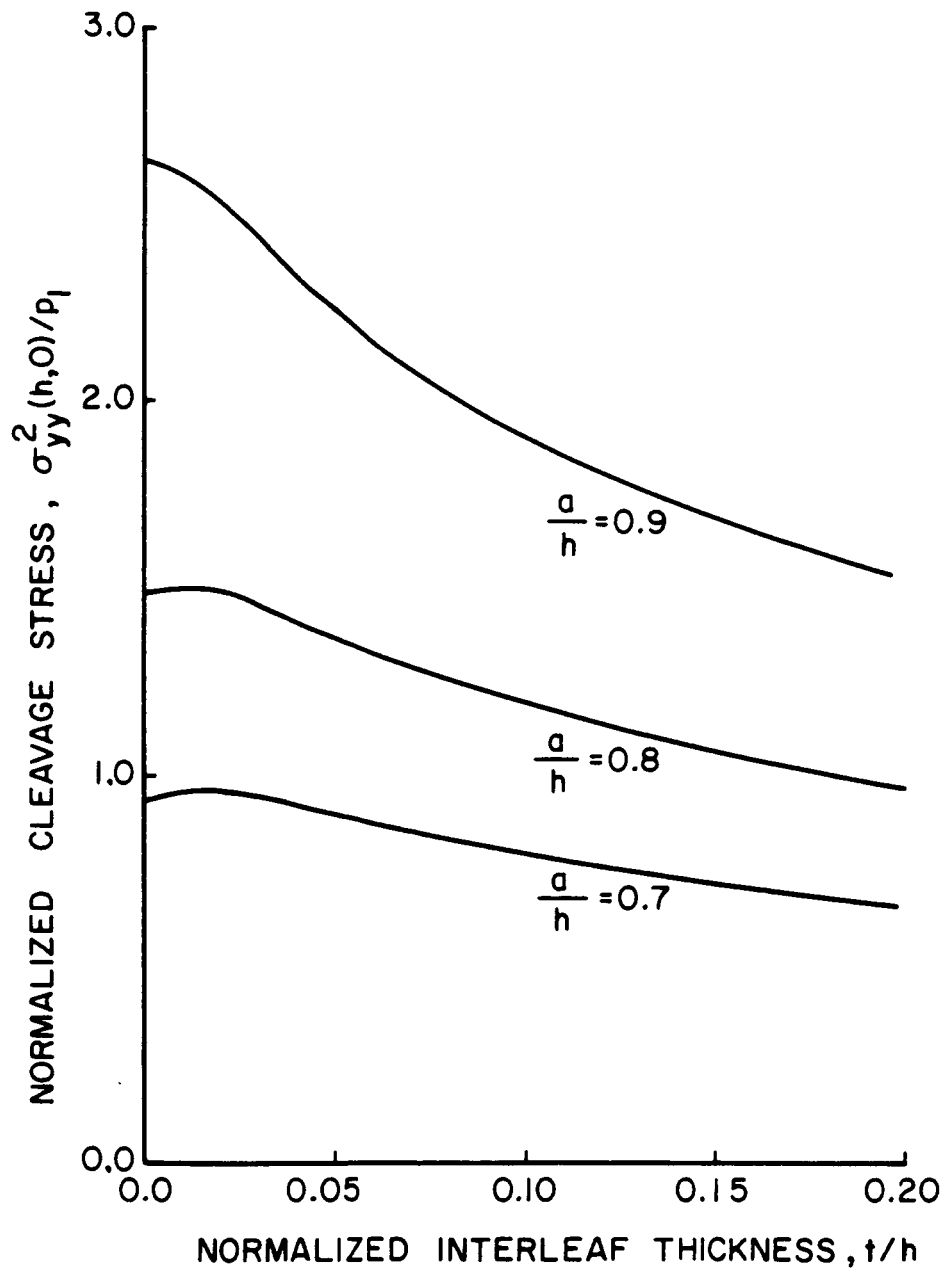


Figure 6. Maximum Cleavage Stress in the Half-Plane as a Function of Interleaf Thickness for Constant Crack Length (MC I)

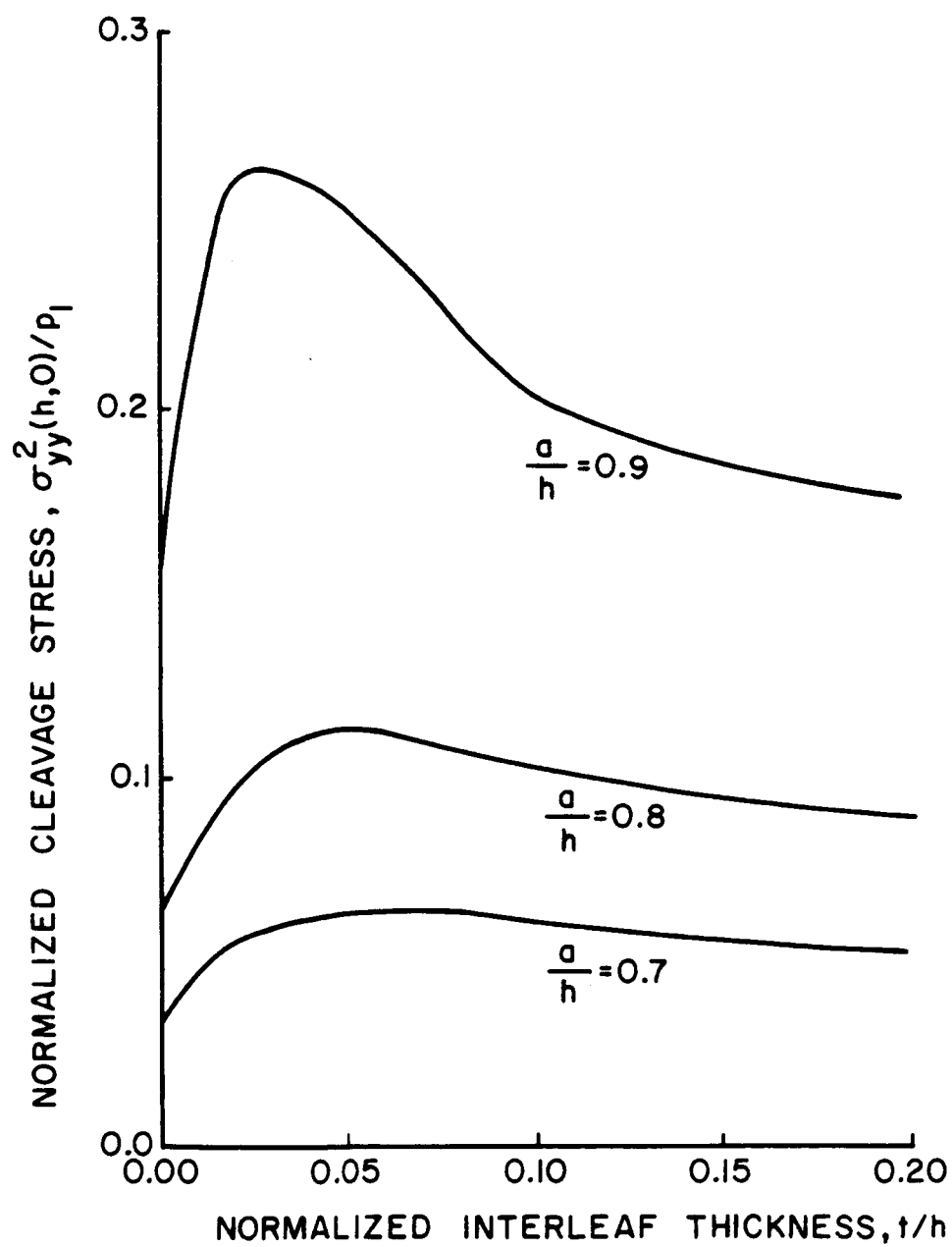


Figure 7. Maximum Cleavage Stress in the Half-Plane as a Function of Interleaf Thickness for Constant Crack Length (MC V)

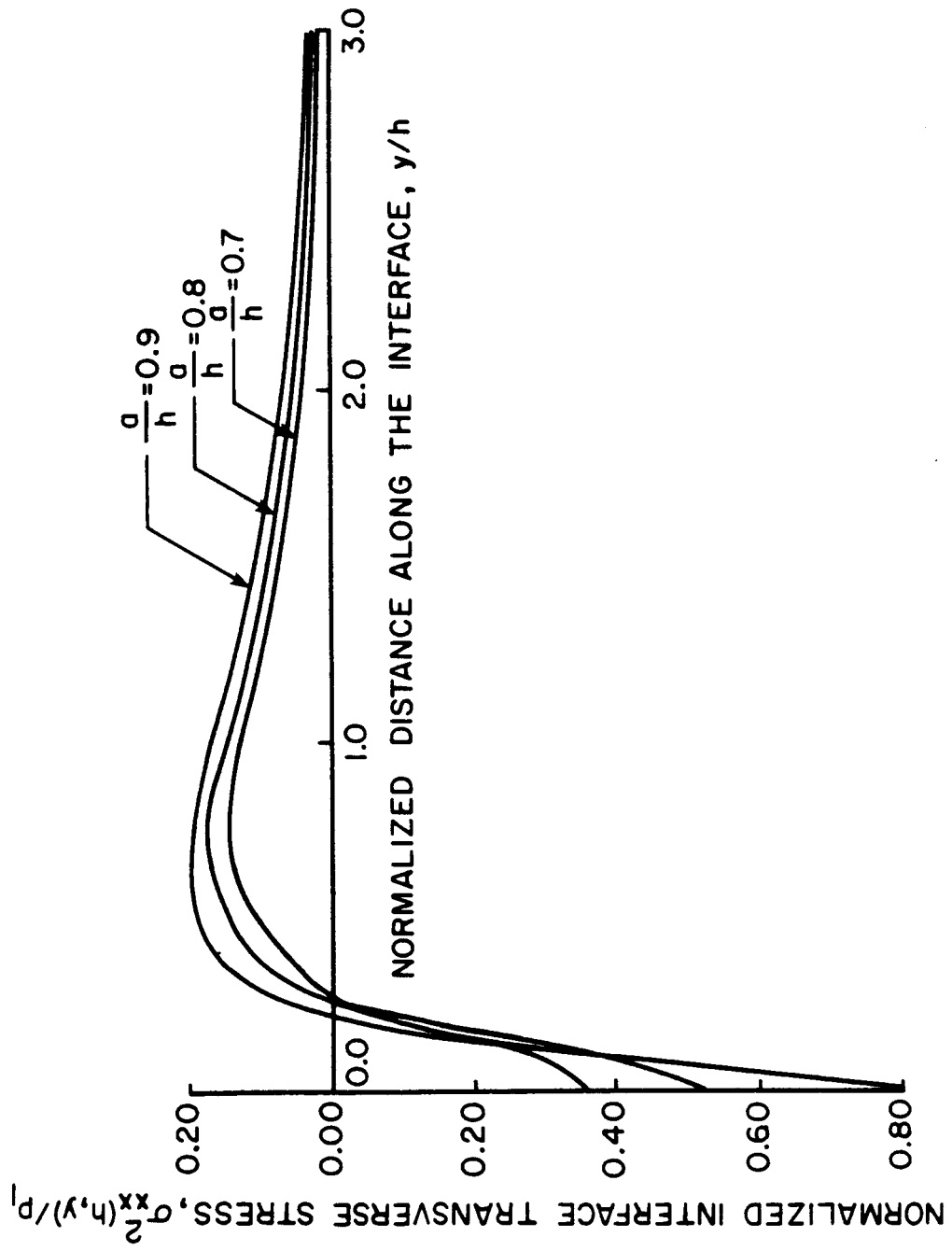


Figure 8. Transverse Stress Distribution Along the Interface for Constant Crack Length (MC I)

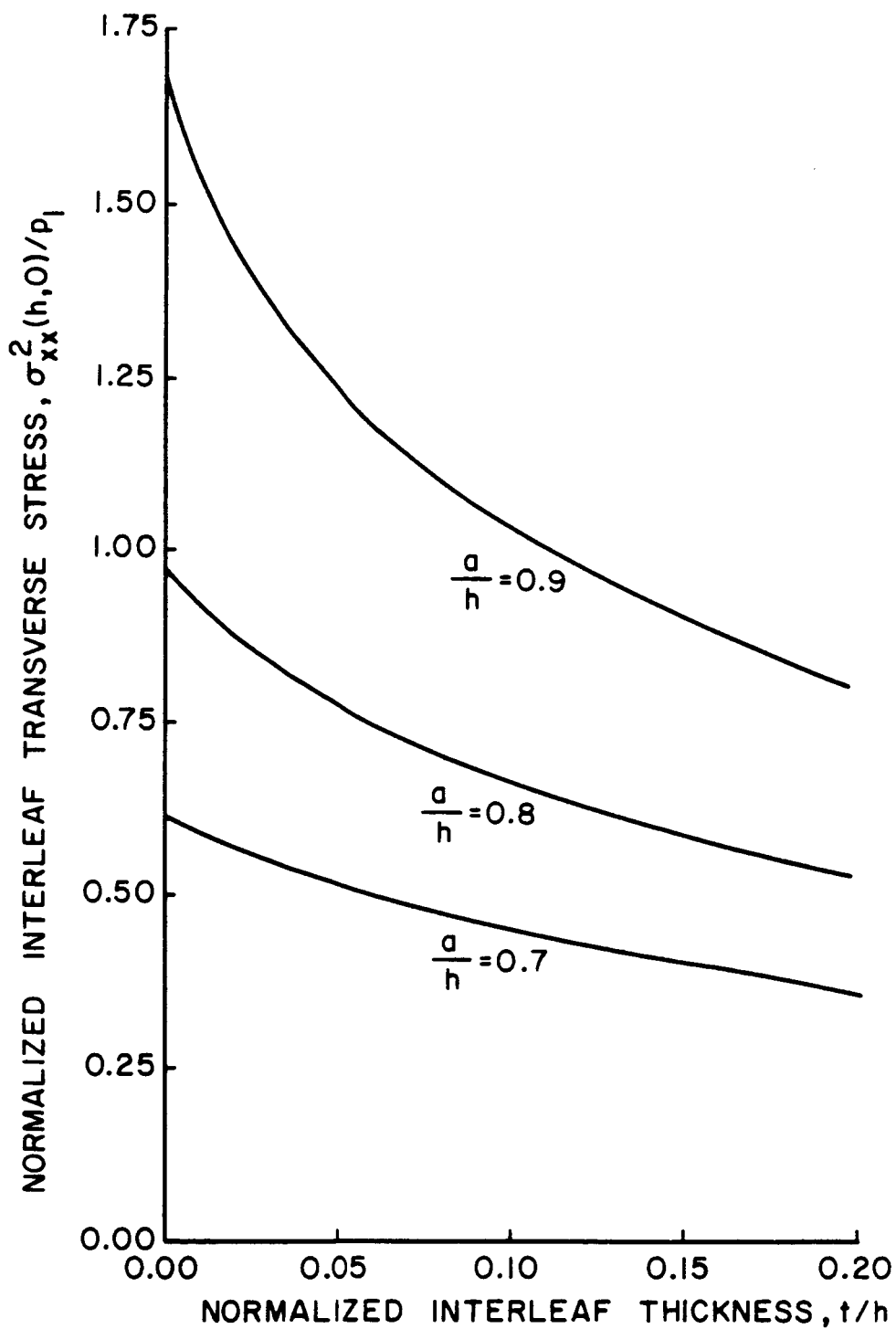


Figure 9. Maximum Interleaf Transverse Stress as a Function of Interleaf Thickness for Constant Crack Length (MC I)

Table II. Maximum interleaf transverse stress for different material combinations ($a/h = 0.9$).

Material Combination	Maximum Interleaf Transverse Stress, $\sigma_{xx}^2(h,0)/p_1$			
	$t/h = 0.0$	0.1	0.2	0.4
MC I	1.6889	1.0358(39)	0.7997(52)	0.5776(66)
MC III	1.2942	0.8753(32)	0.7015(46)	0.5239(60)
MC IV	1.2942	0.2222(83)	0.1350(90)	0.0783(94)
MC V	0.3025	0.1272(58)	0.0893(71)	0.0581(81)

Table III. Maximum interleaf shear stress for different material combinations ($a/h = 0.9$).

Material Combination	Maximum Interleaf Shear Stress, $ \sigma_{xy}^2(h,y) _{\max}/p_1$			
	$t/h = 0$	0.1	0.2	0.4
MC I	0.4845	0.3008(38)	0.2404(50)	0.1800(63)
MC III	0.3184	0.2363(26)	0.1996(37)	0.1571(51)
MC IV	0.3184	0.0741(77)	0.0472(85)	0.0285(91)
MC V	0.1168	0.0374(68)	0.0282(76)	0.0196(83)

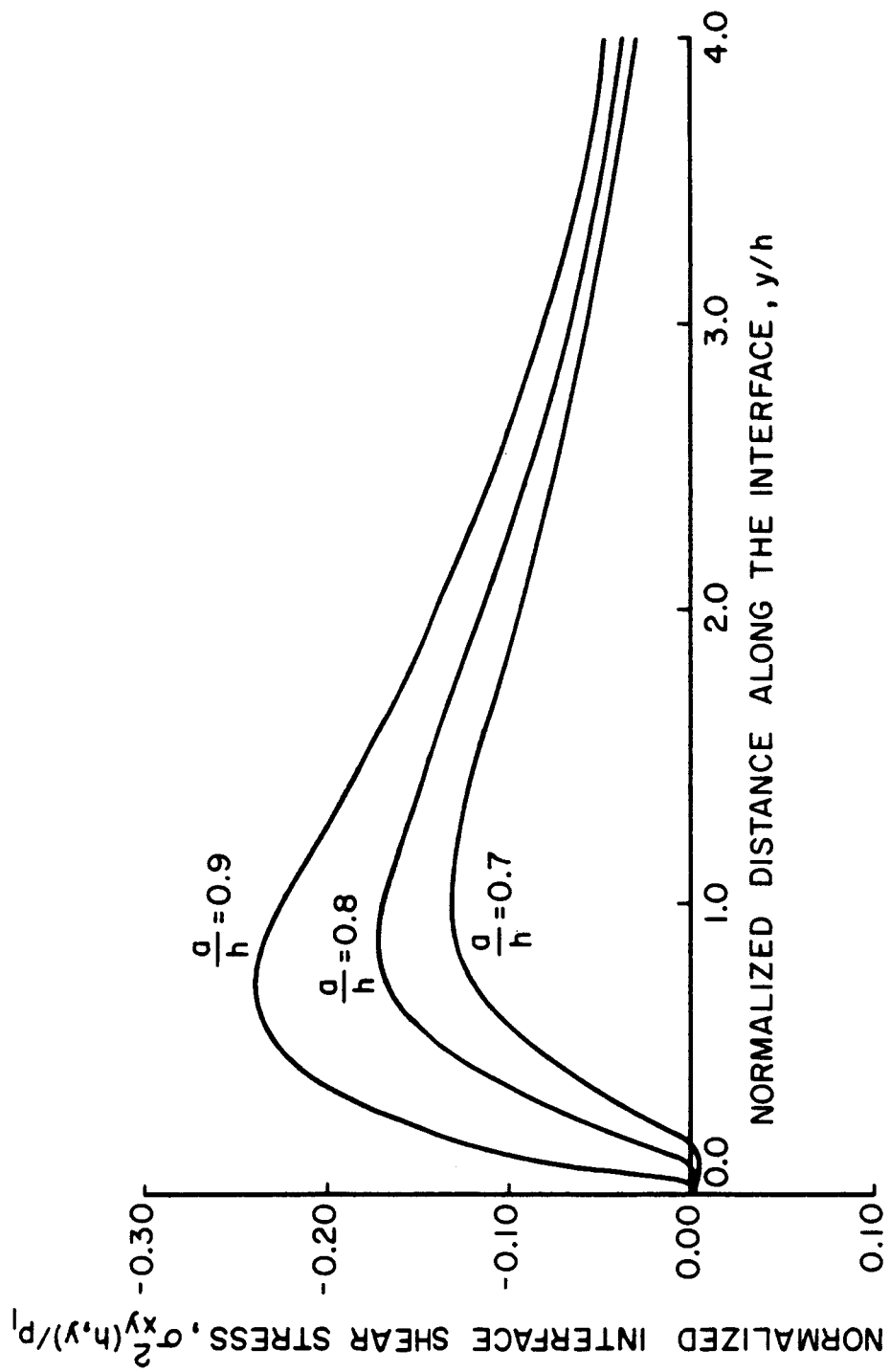


Figure 10. Shear Stress Distribution Along the Interface for Constant Crack Length (MC I)

like the maximum interleaf transverse stress, is a decreasing function of interleaf thickness and is plotted in Figure 11 for MC I. Table III shows the same behavior for all material combinations. The percentage decrease due to the introduction of the interleaf is given in parentheses.

Crack Up to the Interface

The only difference between this and the previous case is that the symmetric crack is now extended up to the interface and represents a broken layer. Due to the interleaf being modeled as a spring, the axial stress in the half-plane for this case has a logarithmic singularity at the crack-tip. A modified stress intensity factor, \tilde{K} is defined by the coefficient of this singularity and is given by equation (103).

Figure 12 shows that this modified stress intensity factor \tilde{K} decreases as a function of increasing interleaf thickness. This decrease is rapid up to $t/h = 0.3$. The modified stress intensity factor, \tilde{K} , unlike the stress intensity factor, K_1 for the crack within the layer, does not directly give a measure of the load carrying capacity from the linear elastic fracture mechanics point of view. It may be recalled that modeling the adhesive as a spring resulted in a logarithmically singular axial stress in the half-plane at the crack-tip. A continuum model would give a power singularity but also not of a square-root type [10]. One of the methods to determine the strength of the composite in such cases is to use failure criteria based on average stresses or point stresses and compare them with the ultimate strength of the undamaged material. A measure of the axial stresses at a specific point $x = 1.01h$ in the half-plane as well as the average stresses calculated

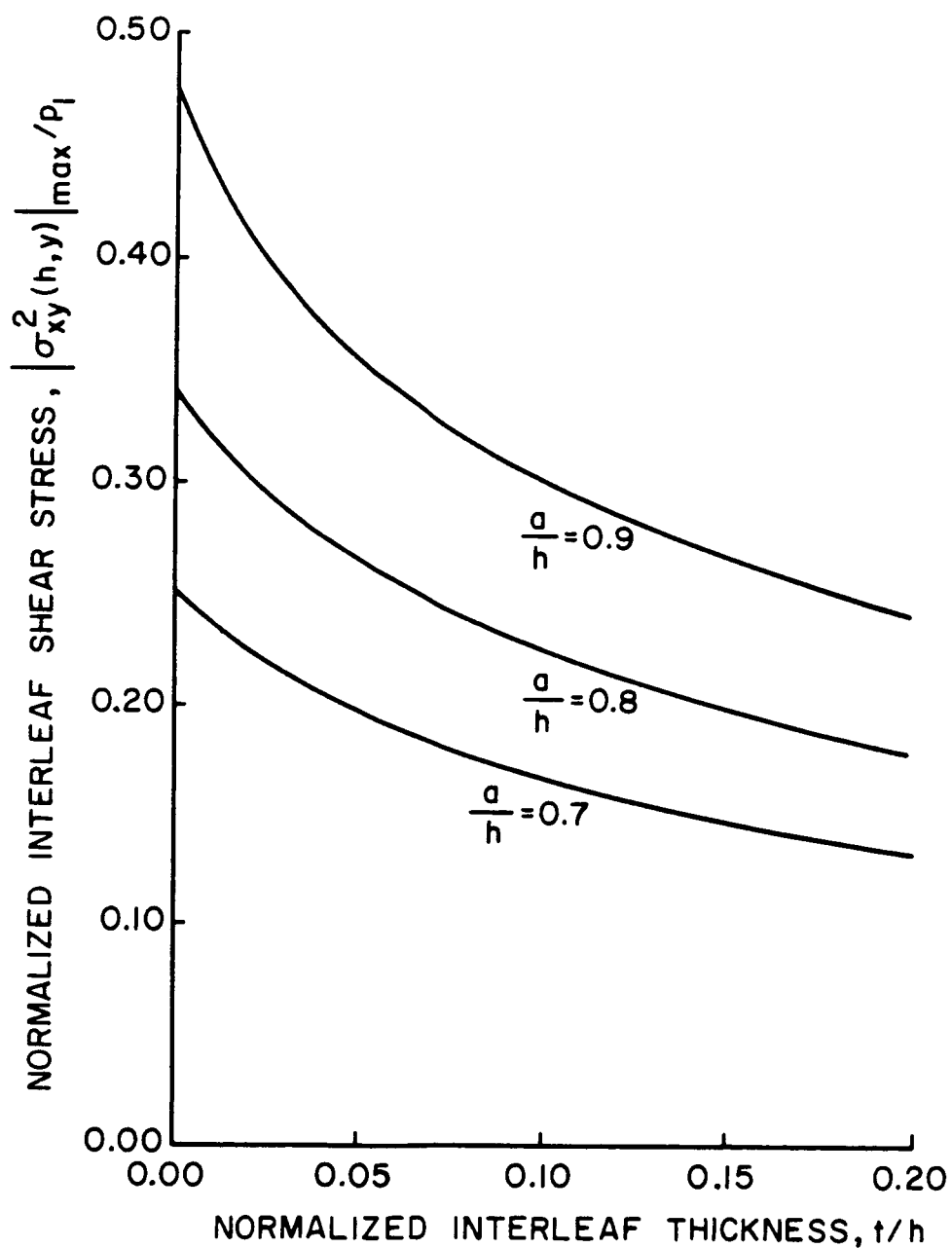


Figure 11. Maximum Interleaf Shear Stress as a Function of Interleaf Thickness for Constant Crack Length (MC I)

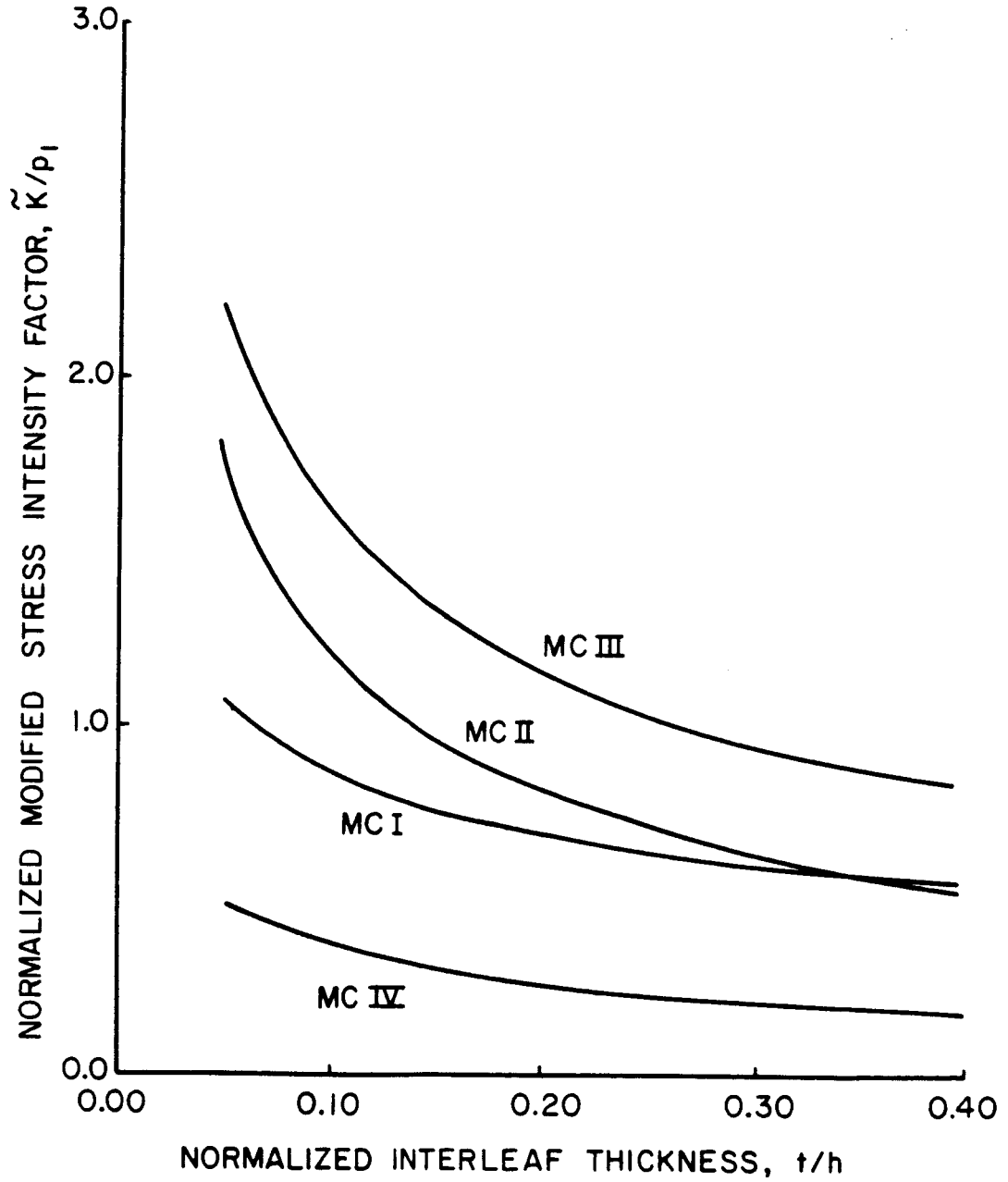


Figure 12. Modified Stress Intensity Factor as a Function of Interleaf Thickness for Different Material Combinations

over the interval $x = h$ to $1.01h$ in the half-plane showed the same behavior of a rapid decrease as the interleaf thickness is increased to $t/h = 0.3$. From the above observations and noting that the interleaves have an insignificant load carrying capacity and add to the weight of the structure, an interleaf thickness of approximately fifteen percent of the layer thickness seems suitable. It may be mentioned that graphite, epoxy and the interleaf have densities of the same order (0.5 pounds/cubic inch).

H-Shaped Crack

In this case, a symmetric transverse crack extending up to the interface and symmetric delamination along the interface is considered as shown in Figure 2. The axial stresses in the half-plane and the layer are, for this case, logarithmically singular at the interface crack-tips and are given by equations (151) and (153). Since the interleaf is modeled as springs, the transverse and shear stresses are finite in the interleaf even at the crack-tip.

Figure 13 plots the transverse and shear stresses at the interface crack-tip, ($x = h$, $y = c$) as a function of split length for MC I. The transverse stress is tensile for no split and decreases rapidly as the splitting is initiated and grows. This peel (transverse) stress becomes compressive and therefore closes the split for relatively small split lengths. On the other hand, the interleaf shear stress at the interface crack-tip shows a very slow continued increase with split length growth. These results indicate that the split tip closes early and that most of the interface crack growth is due to shear alone. It is also found that the split length at which the crack closes decreases as the interleaf thickness is increased. The same behavior is exhibited for all material combinations. However, the order of the split length for the split to

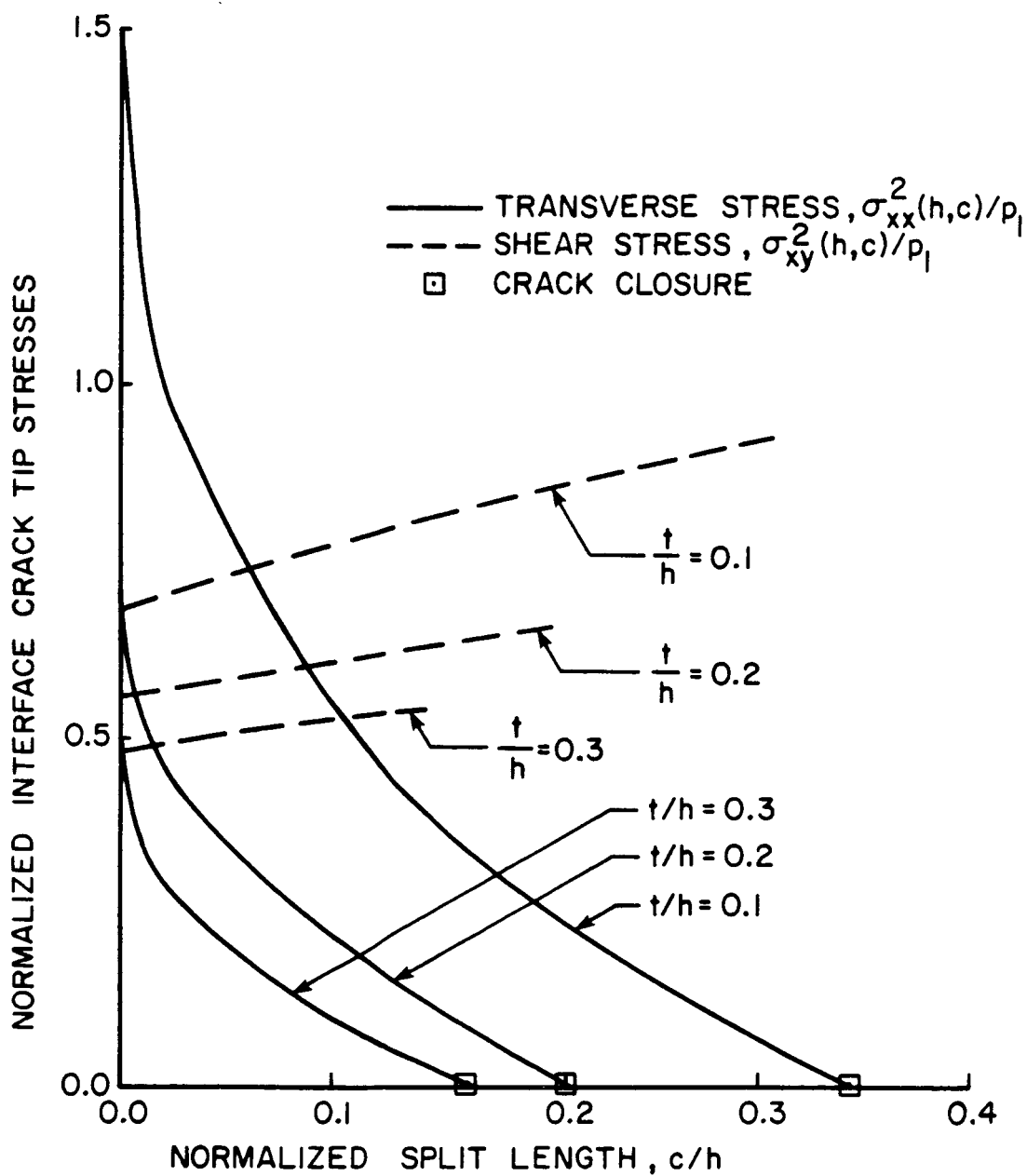


Figure 13. Transverse and Shear Stresses at the Interface Crack-Tip as a Function of Split Length for Constant Interleaf Thickness (MC I)

close varies considerably for each material combination and is illustrated in Table IV. The results are also compared with those obtained by the authors using the formulation and computer code developed by Goree and Venezia [12] for the case of two bonded half-planes with a transverse crack and delamination (T-shaped crack) along the interface. A further discussion on this behavior for longitudinal splitting is presented by Wolla and Goree [29].

Table IV. Length of delamination until closure of crack for different material combinations.

Material Combination	Split Length Until Closure of Crack, c/h		
	$t/h = 0.1$	$t/h = 0.2$	Results from [12]
MC I	0.35	0.21	0.260
MC II	0.018	0.004	0.096
MC III	0.205	0.13	0.164
MC IV	-----	<0.002	0.164

The above results indicate that for a crack in the strong plies (MC II, MC IV), delamination (or at least positive peel stresses) is suppressed very early after initiation. For a crack in the weak plies (MC I, MC III), the extent of delamination is significant and suggests the need for the interleaves as well as that the bond-to-ply interfaces be of high tensile and shear strength. Also, from Figure 13 for zero

split length, the interleaf transverse and shear stresses at the interface crack-tip decrease with an increase in the interleaf thickness. This implies that a thicker interleaf will increase the external load required to initiate delamination. The same behavior is exhibited for all material combinations.

Comparison with Experimental Studies

Although results from a detailed experimental investigation are not available for direct comparison with the analytically predicted results, the preliminary experimental studies done by Masters [1] and Sun [2] are helpful in comparing the behavior of composite laminates with interleaves. These results support the analytically predicted behavior. Sun [2] used a baseline laminate specimen AS4/3501-6 Graphite/Epoxy ($0_5/90_5/0_5$) and placed 5 mil adhesive film (FM1000 by American Cyanamid) between the 0° and 90° plies. The impact velocity required to initiate delamination in the adhesive layered (interleaf) laminate was twice as large as that required for the baseline laminate. Similar results were reported by Masters [1] for the AS4/1808 Graphite/Epoxy laminate $[(\pm 45/0/90/0/90)_2/\pm 45/0/90/\pm 45]_S$. Figure 14 in reference [1], and reproduced here as Figure 14, shows the photomicrographs of the transverse cracks developed in the 90° plies of a baseline and an interleaved laminate. For the same impact loads, the interleaved laminate showed no delamination and damage was limited to transverse cracks. Delaminations occurred only for higher loads but were smaller than the ones developed for baseline laminates at comparable energy levels.



BASELINE LAMINATE (200 X)



INTERLAYERED LAMINATE (200 X)

Figure 14. Transverse Cracks in Baseline and Interlayered AS4/1808 Laminates at an Impact Energy Level of 800 in-lb/in (Reproduced from [1] by permission of Mr. John E. Masters, American Cyanamid Company, Stamford, CT 06904)

CHAPTER IV
CONCLUSIONS

An analytical study is carried out to assist in the understanding of the influence of interleaves on the damage tolerance of multi-layered composite laminates. The geometry of the problem is idealized as a damaged layer bonded to two half-planes and separated by thin interleaves. The interleaves are modeled as distributed tension and shear springs. The damage in the layer is a symmetric transverse crack, which may extend up to the interface. Delamination along the interface is also analyzed. Material combinations assumed to approximate Graphite/Epoxy laminates interlayered with thin thermoplastic film are used to discuss the results. The following conclusions are drawn from the study.

A. For the case of a crack within the layer:

- 1) The stresses at the crack-tip are singular and have, as expected, the classical square root singularity.
- 2) The introduction of the low modulus interleaves increases the potential for the crack to extend while it is within the layer but reduces the stresses at the interface, which improves delamination damage tolerance.
- 3) If the crack is in a layer which is stiffer than the half-planes, the use of interleaves results in higher cleavage stresses in the half-plane and may assist in continuing the crack across the interface.

B. For the case of a crack up to the interface:

- 4) By modeling the interleaves as distributed tension and shear springs, the axial stress in the half-planes is logarithmically singular at the crack-tip.
- 5) The stresses in the interleaves and the half-planes reduce with an increase in the interleaf thickness. The rate of this reduction is most rapid for small interleaf thicknesses. For example, for the material combinations

of interleaved Graphite/Epoxy used in the results, this thickness is of the order of fifteen percent of the layer thickness. Any further increase in the thickness of the interleaf is an unprofitable addition to structural weight.

C. For the case of an H-shaped crack:

- 6) The axial stresses in the layer and the half-planes at the interface crack-tip are logarithmically singular, whereas the axial stresses in the half-planes at the intersecting points of the interface cracks and the transverse crack are bounded.
- 7) The growth of delamination along the interface is stable. The split tip closes as the transverse stresses become compressive for small split lengths and further growth is due to shear alone.
- 8) The split length until the split tip closes decreases with an increase in the interleaf thickness (or decrease in interleaf moduli).

Based on the above conclusions, an interleaf thickness of the order of fifteen percent of the layer width is recommended for typical Graphite/Epoxy laminates. Since transverse cracks are more likely to occur in weak plies, the weak-stiff ply interfaces are prone to high stresses, which makes interleaving such interfaces a first choice. Similarly, the weak-weak ply interfaces are also prone to higher stresses but the possibility of a crossover of the transverse crack is also high. This makes interleaving such interfaces a secondary choice.

APPENDICES

Appendix AIntegral Expressions and Limit Evaluations

The following integral formulas and limit evaluations [8, 27, 30] are used in the formulation:

$$\frac{d^m}{dr^m} \int_0^{\infty} e^{-ry} \cos(ys) dy = \frac{d^m}{dr^m} \left[\frac{r}{r^2 + s^2} \right], \quad r > 0,$$

$$\frac{d^m}{dr^m} \int_0^{\infty} e^{-ry} \sin(ys) dy = \frac{d^m}{dr^m} \left[\frac{s}{r^2 + s^2} \right], \quad r > 0,$$

$$\int_0^{\infty} \frac{1}{r(r^2 + s^2)} \sin(ry) dr = \frac{\pi}{2s^2} (1 - e^{-sy}),$$

$$\int_0^{\infty} \frac{r}{(r^2 + s^2)^2} \sin(ry) dr = \frac{\pi}{4s} y e^{-sy},$$

$$\int_0^{\infty} \frac{1}{r^2 + s^2} \cos(ry) dr = \frac{\pi}{2s} e^{-sy},$$

$$\int_0^{\infty} \frac{s^2}{(r^2 + s^2)^2} \cos(ry) dr = \frac{\pi}{4s} (1 + sy) e^{-sy},$$

$$\int_0^{\infty} \frac{r^2}{(r^2 + s^2)^2} \cos(ry) dr = \frac{\pi}{4s} (1 - sy) e^{-sy},$$

$$\int_0^{\infty} e^{-ry} \cos rx \sin rt dr = \frac{1}{2} \left[\frac{t - x}{(t - x)^2 + y^2} + \frac{t + x}{(t + x)^2 + y^2} \right], \quad y > 0,$$

$$\int_0^{\infty} e^{-ry} \cos rx \cos rt \, dr = \frac{1}{2} \left[\frac{y}{(t-x)^2 + y^2} + \frac{y}{(t+x)^2 + y^2} \right], \quad y > 0,$$

$$\int_0^{\infty} e^{-ry} \sin rx \sin rt \, dr = \frac{1}{2} \left[\frac{y}{(t-x)^2 + y^2} - \frac{y}{(t+x)^2 + y^2} \right], \quad y > 0.$$

Let a function $f(t)$ be continuous on L and satisfy the Holder conditions on $L + L'$, then

$$\lim_{x \rightarrow 0} \int_0^{\infty} f(t) \left[\frac{x}{x^2 + (t-y)^2} \right] \pm \frac{x}{x^2 + (t+y)^2} \, dt = \pi f(y),$$

$$\lim_{x \rightarrow 0} \int_0^{\infty} f(t) \left\{ \frac{x^3 - x(t-y)^2}{[x^2 + (t-y)^2]^2} \pm \frac{x^3 - x(t+y)^2}{[x^2 + (t+y)^2]^2} \right\} dt = 0,$$

$$\lim_{x \rightarrow 0} \int_0^{\infty} f(t) \left\{ \frac{x^2(t+y)}{[x^2 + (t+y)^2]^2} - \frac{x^2(t-y)}{[x^2 + (t-y)^2]^2} \right\} dt = 0,$$

everywhere except at the end points of L .

Appendix B

Definition of Constants

The functions a_{ij} , ($i = 1, \dots, 4$, $j = 1, \dots, 4$), and D_i , ($i = 1, \dots, 4$), in equation (24) are

$$a_{11} = -\text{Cosh } \eta h,$$

$$a_{12} = -\eta h \text{ Sinh } \eta h,$$

$$a_{13} = a_{14} = \frac{\mu_2}{\mu_1} e^{-\eta h},$$

$$a_{21} = \text{Sinh } \eta h,$$

$$a_{22} = \text{Sinh } \eta h + \eta h \text{ Cosh } \eta h,$$

$$a_{23} = \frac{\mu_2}{\mu_1} e^{-\eta h},$$

$$a_{24} = (\eta h - 1) \frac{\mu_2}{\mu_1} e^{-\eta h},$$

$$a_{31} = -\text{Sinh } \eta h,$$

$$a_{32} = \frac{\kappa_1 - 1}{2} \text{ Sinh } \eta h - \eta h \text{ Cosh } \eta h,$$

$$a_{33} = -\frac{2\mu_2 t}{E_0} \eta - 1,$$

$$a_{34} = \left[-\frac{2\mu_2 t}{E_0} \eta^2 h - \frac{\kappa_2 - 1}{2} - \eta h \right] e^{-\eta h},$$

$$a_{41} = -\text{Cosh } \eta h,$$

$$a_{42} = -\frac{\kappa_1 + 1}{2} \text{ Cosh } \eta h - \eta h \text{ Sinh } \eta h,$$

$$a_{43} = \left[\frac{2\mu_2 t \eta}{\mu_3} + 1 \right] e^{-\eta h},$$

$$a_{44} = \left[\frac{2\mu_2 t \eta}{\mu_3} (\eta h - 1) - \frac{\kappa_2 + 1}{2} + \eta h \right] e^{-\eta h}.$$

$$D_1(\eta) = \frac{4\eta^2}{\pi} \int_0^{\infty} \frac{\xi \phi_1(\xi)}{(\xi^2 + \eta^2)^2} \cos \xi h \, d\xi,$$

$$D_2(\eta) = \frac{4\eta}{\pi} \int_0^{\infty} \frac{\xi^2 \phi_1(\xi)}{(\xi^2 + \eta^2)^2} \sin \xi h \, d\xi,$$

$$D_3(\eta) = \frac{2\eta}{\pi} \int_0^{\infty} \frac{\phi_1(\xi)}{(\xi^2 + \eta^2)^2} \left[\left(\frac{\kappa_1 - 3}{2} \right) (\xi^2 + \eta^2) + 2\eta^2 \right] \sin \xi h \, d\xi,$$

$$D_4(\eta) = \frac{2\eta^2}{\pi} \int_0^{\infty} \frac{\phi_1(\xi)}{\xi(\xi^2 + \eta^2)^2} \left[\left(\frac{\kappa_1 + 1}{2} \right) (\xi^2 + \eta^2) + 2\xi^2 \right] \cos \xi h \, d\xi.$$

The expressions for the functions α_{ij} , ($i = 1, 2$, $j = 1, 2$) in equation (25) are

$$\alpha_{11} = \left[\frac{\eta}{2}(\lambda_3 + \lambda_4) + 1 \right] + \left[\frac{\eta}{2}(\lambda_3 - \lambda_4) \right] e^{-2\eta h},$$

$$\alpha_{12} = \left[\frac{\eta^2 h}{2}(\lambda_3 + \lambda_4) + \frac{\lambda_4 \eta}{2} + \eta h + \frac{1}{2} \right]$$

$$+ \left[\frac{\eta^2 h}{2}(-\lambda_3 + \lambda_4) - \frac{\lambda_4 \eta}{2} + \frac{\lambda_1}{2} \right] e^{-2\eta h},$$

$$\alpha_{21} = \left[\frac{\eta}{2}(-\lambda_5 + \lambda_6) \right] + \left[\frac{\eta}{2}(-\lambda_5 - \lambda_6) + \lambda_2 \right] e^{-2\eta h},$$

$$\alpha_{22} = \left[\frac{\eta^2 h}{2}(-\lambda_5 + \lambda_6) + \frac{\lambda_6 \eta}{2} + \frac{1}{2} \right]$$

$$+ \left[\frac{\eta^2 h}{2}(\lambda_5 + \lambda_6) - \lambda_2 \eta h - \frac{\lambda_6 \eta}{2} + \frac{\lambda_2}{2} \right] e^{-2\eta h},$$

where the material constants λ_i , ($i = 1, \dots, 6$), are expressed as

$$\lambda_1 = \frac{\kappa_1 \mu_2 - \kappa_2 \mu_1}{\mu_2 + \kappa_2 \mu_1},$$

$$\lambda_2 = \frac{\mu_2 - \mu_1}{\mu_1 + \kappa_1 \mu_2},$$

$$\lambda_3 = \frac{2\mu_1 \mu_2}{K_N(\kappa_2 \mu_1 + \mu_2)},$$

$$\lambda_4 = \frac{2\mu_1 \mu_2}{K_S(\kappa_2 \mu_1 + \mu_2)},$$

$$\lambda_5 = \frac{2\mu_1 \mu_2}{K_N(\kappa_1 \mu_2 + \mu_1)},$$

$$\lambda_6 = \frac{2\mu_1 \mu_2}{K_S(\kappa_1 \mu_2 + \mu_1)}.$$

The above material constants are related by

$$\lambda_3(\lambda_2 + 1) = \lambda_5(\lambda_1 + 1),$$

$$\lambda_3 \lambda_6 = \lambda_4 \lambda_5,$$

which implies that there are four independent composite parameters. The dependence of the solution can hence be studied as a function of only four composite parameters. This concept has been discussed in detail by Dundurs [31].

The expressions for the functions F_i , ($i = 1, 2$), in equation (29) are

$$F_1(\eta) = -\lambda_3 \eta D_1 + \lambda_4 \eta D_2 - \frac{\kappa_2 \mu_1}{\kappa_2 \mu_1 + \mu_2} (D_1 - D_2) - \frac{\mu_2}{\kappa_2 \mu_1 + \mu_2} (D_3 + D_4),$$

$$F_2(\eta) = \lambda_5 \eta D_1 + \lambda_6 \eta D_2 + \frac{\mu_1}{\kappa_1 \mu_2 + \mu_1} (D_1 + D_2) + \frac{\mu_2}{\kappa_1 \mu_2 + \mu_1} (D_3 - D_4).$$

The expressions for the functions $H_i(\eta, t)$, ($i = 1, \dots, 4$), in equation (28) are

$$H_1(\eta, t) = \eta[1 - \eta(h - t)],$$

$$H_2(\eta, t) = \eta[2 - \eta(h - t)],$$

$$H_3(\eta, t) = \eta \left[\eta(h - t) + \frac{\kappa_1 - 3}{2} \right],$$

$$H_4(\eta, t) = \eta \left[-\eta(h - t) + \frac{\kappa_1 + 3}{2} \right].$$

The integrands E_i , ($i = 1, 2$), in equation (29) are

$$E_1(\eta, t) = \frac{1}{\kappa_1 + 1} \left[\eta^3(h - t) (\lambda_3 - \lambda_4) + \eta^2(2\lambda_4 - \lambda_3) - \lambda_1\eta \right],$$

$$E_2(\eta, t) = \frac{1}{\kappa_1 + 1} \left[\eta^3(h - t) (-\lambda_5 - \lambda_6) + \eta^2(\lambda_5 + 2\lambda_6) \right. \\ \left. + 2\eta^2(h - t) \lambda_2 - 3\lambda_2\eta \right].$$

The functions f_{11} and f_{22} in equation (38) are

$$f_{11} = [-\lambda_1 + \lambda_4\eta] + [(-2\lambda_3 + 2\lambda_4)\eta^2h - \lambda_4\eta + \lambda_1] e^{-2\eta h},$$

$$f_{22} = [-\lambda_2 + \lambda_6\eta] + [(2\lambda_5 + 2\lambda_6)\eta^2h - 4\lambda_2\eta h - \lambda_6\eta + \lambda_2] e^{-2\eta h}.$$

The material constants in equations (65) and (69) are

$$B_1 = C_2 + 4C_6,$$

$$B_2 = C_5 - 2C_6,$$

$$B_3 = 2C_3 + 4C_7 - C_2C_6 - 4C_6^2,$$

$$B_4 = C_4 - 6C_6,$$

$$B_5 = C_8 - 4C_6,$$

$$B_6 = -C_6 + \sqrt{C_6^2 - 4C_7},$$

where

$$C_2 = \frac{2}{\lambda_3\lambda_6} (-\lambda_5 - \lambda_6 + \lambda_2\lambda_3 + \lambda_2\lambda_4),$$

$$C_3 = \frac{2\lambda_2}{\lambda_3\lambda_6},$$

$$C_4 = \frac{1}{\lambda_3\lambda_6} (-\lambda_3 + \lambda_4 + 3\lambda_5 + 3\lambda_6 - 4\lambda_2\lambda_3 - 2\lambda_2\lambda_4),$$

$$C_5 = \frac{1}{\lambda_3 \lambda_6} (-\lambda_1 \lambda_5 + \lambda_1 \lambda_6 + 2\lambda_6 - \lambda_2 \lambda_3 - \lambda_2 \lambda_4),$$

$$C_6 = \frac{1}{2\lambda_3 \lambda_6} (\lambda_3 + \lambda_4 + \lambda_5 + \lambda_6),$$

$$C_7 = \frac{1}{\lambda_3 \lambda_6},$$

$$C_8 = \frac{1}{\lambda_3 \lambda_6} (\lambda_4 - 2\lambda_1 \lambda_5 + \lambda_1 \lambda_6 + 3\lambda_6 - 2\lambda_2 \lambda_3 - \lambda_2 \lambda_4).$$

The right hand sides of equations (126) are given by

$$L_1(\eta) = D_1(\eta),$$

$$L_2(\eta) = D_2(\eta),$$

$$L_3(\eta) = D_3(\eta) + \frac{2\mu_1 \eta}{K_n(\kappa_1 + 1)} \int_0^{\infty} \phi_2(y) \cos \eta y \, dy,$$

$$L_4(\eta) = D_4(\eta) + \frac{2\mu_1 \eta}{K_s(\kappa_1 + 1)} \int_0^{\infty} \phi_3(y) \sin \eta y \, dy,$$

and in terms of finite integrals as

$$(\kappa_1 + 1) L_1(\eta) = \int_{-h}^h v(t) H_1(\eta, t) e^{-\eta(h-t)} \, dt,$$

$$(\kappa_1 + 1) L_2(\eta) = \int_{-h}^h v(t) H_2(\eta, t) e^{-\eta(h-t)} \, dt,$$

$$(\kappa_1 + 1) L_3(\eta) = \int_{-h}^h v(t) H_3(\eta, t) e^{-\eta(h-t)} \, dt \\ + \frac{2\mu_1 \eta}{K_n} \int_0^c \phi_2(y) \cos \eta y \, dy,$$

$$(\kappa_1 + 1) L_4(\eta) = \int_{-h}^h v(t) H_4(\eta, t) e^{-\eta(h-t)} \, dt \\ + \frac{2\mu_1 \eta}{K_s} \int_0^c \phi_3(y) \sin \eta y \, dy,$$

The expressions for N_i , ($i = 1, 2$), in equation (143) are

$$N_1 = -2 + \frac{(\lambda_6 - \lambda_3 - \lambda_4 - \lambda_5)(h - x)}{2\lambda_3\lambda_6},$$

$$N_2 = -2 + \frac{(\lambda_6 - \lambda_3 - \lambda_4 - \lambda_5)(h + x)}{2\lambda_3\lambda_6}.$$

The expressions for Z_{ij} , ($i = 1, 2, 3$, $j = 1, 2, 3$), in equations (159-161) are

$$Z_{11}(k, r) = \frac{-2(k+1)}{1-r^2} \{r Q_k(r) - Q_{k+1}(r)\} \\ + \int_{-1}^1 h^2 K_{11}(hs, hr) P_k(s) ds, \quad (k=0, 1, \dots, K-1, K),$$

$$Z_{12}(\ell, r) = \frac{1}{2} \int_{-1}^1 c^2 K_{12}(hr, cw) T_\ell(w) dw, \quad (\ell=0, 1, \dots, L-1, L),$$

$$Z_{13}(0, r) = \frac{1}{2} \int_{-1}^1 c^2 K_{13}(hr, cw) \text{sign}(w) dw,$$

$$Z_{13}(m, r) = \frac{1}{2} \int_{-1}^1 c^2 K_{13}(hr, cw) T_m(w) dw, \quad (m=1, 2, \dots, M-1, M),$$

$$Z_{21}(k, q) = \int_{-1}^1 h^2 K_{21}(cq, hs) P_k(s) ds, \quad (k=0, 1, \dots, K-1, K),$$

$$Z_{22}(\ell, q) = \frac{1}{2} \left[\int_{-1}^1 c^2 K_{22}(cq, cw) T_\ell(w) dw - \pi c \right], \quad (\ell=0, 1, \dots, L-1, L),$$

$$Z_{23}(0, q) = \frac{1}{2} \int_{-1}^1 c^2 K_{23}(cq, cw) \text{sign}(w) dw,$$

$$Z_{23}(m, q) = \frac{1}{2} \int_{-1}^1 c^2 K_{23}(cq, cw) T_m(w) dw, \quad (m=1, 2, \dots, M-1, M),$$

$$Z_{31}(k,q) = \int_{-1}^1 h^2 K_{31}(cq, hs) P_k(s) ds, \quad (k=0,1,\dots,K-1,K),$$

$$Z_{32}(\ell,q) = \frac{1}{2} \int_{-1}^1 c^2 K_{32}(cq, cw) T_\ell(w) dw, \quad (\ell=0,1,\dots,L-1,L),$$

$$Z_{33}(0,q) = \frac{1}{2} \left[\int_{-1}^1 c^2 K_{33}(cq, cw) \text{sign}(w) dw - \pi c \text{sign}(q) \right],$$

$$Z_{33}(m,q) = \frac{1}{2} \left[\int_{-1}^1 c^2 K_{33}(cq, cw) T_m(w) dw - \pi c \right], \quad (m=1,2,\dots,M-1,M).$$

Appendix C

Stress Intensity Factor for the Embedded Crack

The stress intensity factor for an embedded crack ($a < h$) is given by equation (61) as

$$K_1 = \lim_{x \rightarrow a^+} \sqrt{2(x-a)} \sigma_{yy}^1(x,0). \quad (61)$$

From equations (30-41), the axial stress $\sigma_{yy}^1(x,0)$ can be written as

$$\sigma_{yy}^1(x,0) = \frac{4\mu_1}{1+\kappa_1} \int_{-a}^a \frac{G(t)}{t-x} dt + \text{bounded function}. \quad (C.1)$$

$G(t)$ has an integrable singularity at $t = \pm a$ given by

$$G(t) = \frac{H(t)}{\sqrt{a^2 - t^2}}, \quad (51)$$

or

$$G(t) = \frac{H(t) e^{\pi i/2}}{(t-a)^{\frac{1}{2}} (t+a)^{\frac{1}{2}}}. \quad (C.2)$$

Consider the sectionally holomorphic function

$$\phi(z) = \int_{-a}^a \frac{G(t)}{t-z} dt. \quad (C.3)$$

According to Muskhelishvili [20, Chapter 4] and using equation (C.2)

$$\phi(z) = \frac{H(-a) e^{i\pi/2}}{\sqrt{2a} \sqrt{z+a}} - \frac{H(a)}{\sqrt{2a} \sqrt{z-a}} + \phi_0(z), \quad (C.4)$$

where $\phi_0(z)$ is a bounded everywhere except at the end points $z = \pm a$,

where

$$|\phi_0(z)| \leq \frac{H_0(\pm a)}{|z \pm a|^{\gamma_0}}, \quad \text{Re}(\gamma_0) < \frac{1}{2}. \quad (C.5)$$

Using the Plemelj formulas (47) on equation (C.4), the function $\phi(x)$ may be defined near $x = a$ by

$$\phi(x) = - \frac{H(a)}{\sqrt{2a} \sqrt{x-a}} + \bar{\phi}_0(x), \quad (C.6)$$

where $\bar{\phi}_0(x)$ is a bounded function and has a behavior similar to $\phi_0(z)$ at the end points. From equations (C.1), (C.3), (C.6), and (61), the value of the mode I stress intensity factor is given by

$$K_1 = - \frac{4 \mu_1}{(1 + \kappa_1)} \frac{H(a)}{\sqrt{a}}, \quad a < h. \quad (C.7)$$

In terms of the non-dimensional function $\Psi(s)$, defined by equation (56), the stress intensity factor, K_1 , can be re-written as

$$K_1 = - \frac{4\mu_1}{(1 + \kappa_1)} \frac{\Psi(1)}{\sqrt{a}}, \quad a < h. \quad (C.8)$$

Appendix D

Cleavage Stress in the Half-Plane
for the Broken Layer

The cleavage stress in the half-plane is given by

$$\sigma_{yy}^2(x,0) = \frac{4\mu_2}{\pi} \int_0^{\infty} [f_2(\eta) + (\eta x - 2)g_2(\eta)] e^{-\eta x} d\eta. \quad (D.1)$$

From equation (24), the functions $f_2(\eta)$ and $g_2(\eta)$ may be expressed as

$$\begin{aligned} \frac{\mu_2}{\mu_1} f_2(\eta) e^{-\eta h} &= f_1(\eta) [-\eta h e^{\eta h} + \text{Cosh } \eta h] + g_1(\eta) [-\eta^2 h^2 e^{\eta h}] \\ &+ (1 - \eta h) D_1 + \eta h D_2, \end{aligned} \quad (D.2)$$

$$\begin{aligned} \frac{\mu_2}{\mu_1} g_2(\eta) e^{-\eta h} &= f_1(\eta) [e^{\eta h}] + g_1(\eta) [\eta h e^{\eta h} + \text{Sinh } \eta h] \\ &+ D_1 - D_2. \end{aligned} \quad (D.3)$$

Substituting equations (D.2), (D.3), and (24) in equation (D.1) for $a = h$,

$$\begin{aligned} \sigma_{yy}^2(x,0) &= \frac{4\mu_1}{\pi(\kappa_1 + 1)} \int_0^{\infty} \int_{-h}^h (\delta_1 \eta^2 + \delta_2 \eta + \delta_3) v(t) e^{-\eta(x-t)} dt d\eta \\ &+ \frac{4\mu_1}{\pi} \int_0^{\infty} \{ [-\eta(h-x) - 1] D_1 \\ &+ [\eta(h-x) + 2] D_2 \} e^{-\eta(x-h)} d\eta \\ &+ \text{bounded function}, \end{aligned} \quad (D.4)$$

where

$$\begin{aligned} \delta_1 &= Q_1(h-t)(h-x) + (h-t) - (h-x), \\ \delta_2 &= -Q_9 Q_1(h-t)(h-x) + (Q_3 - Q_9)(h-t) \\ &+ (Q_4 - Q_9)(h-x) - 3, \end{aligned}$$

$$\begin{aligned}\delta_3 = & (-Q_{10} Q_1 + Q_9^2 Q_1)(h - t)(h - x) \\ & + (Q_5 - Q_{10} - Q_9 Q_3 + Q_9^2)(h - t) \\ & + (Q_6 + Q_{10} - Q_9 Q_4 + Q_9^2)(h - x) \\ & + (Q_7 + 3Q_9).\end{aligned}$$

and

$$Q_1 = \frac{1}{\lambda_3 \lambda_6} (-\lambda_3 + \lambda_4 - \lambda_3 \lambda_2 + \lambda_2 \lambda_4),$$

$$Q_3 = \frac{1}{2\lambda_3 \lambda_6} (-3\lambda_3 + 3\lambda_4 + 2\lambda_2 \lambda_4 - 4\lambda_2 \lambda_3 + \lambda_5 + \lambda_6),$$

$$Q_4 = \frac{1}{2\lambda_3 \lambda_6} (\lambda_1 \lambda_5 + \lambda_1 \lambda_6 - 4\lambda_4 + 2\lambda_3 + 3\lambda_2 \lambda_3 - 3\lambda_2 \lambda_4),$$

$$Q_5 = -\frac{\lambda_2}{\lambda_3 \lambda_6},$$

$$Q_6 = \frac{\lambda_1}{\lambda_3 \lambda_6},$$

$$Q_7 = \frac{1}{2\lambda_3 \lambda_6} (2\lambda_1 \lambda_5 + \lambda_1 \lambda_6 - 6\lambda_4 + 3\lambda_3 - 3\lambda_2 \lambda_4 + 6\lambda_2 \lambda_3 - \lambda_5 - 2\lambda_6),$$

$$Q_8 = \frac{3}{2\lambda_3 \lambda_6} (\lambda_1 + \lambda_2),$$

$$Q_9 = \frac{1}{2\lambda_3 \lambda_6} (\lambda_3 + \lambda_4 + \lambda_5 + \lambda_6),$$

$$Q_{10} = \frac{1}{\lambda_3 \lambda_6}.$$

The values of λ_i , ($i = 1, \dots, 6$), in terms of material constants are given in Appendix B.

Using the following relationships

$$\int_0^{\infty} \eta^m e^{-\eta(x-t)} d\eta = (-1)^m \frac{d^m}{dx^m} \left(\frac{1}{x-t} \right),$$

$$(h-t) \frac{d}{dx} \left(\frac{1}{x-t} \right) = (h-x) \frac{d}{dx} \left(\frac{1}{x-t} \right) - \frac{1}{x-t},$$

C-2

$$(h - t) \frac{d^2}{dx^2} \left(\frac{1}{x - t} \right) = (h - x) \frac{d^2}{dx^2} \left(\frac{1}{x - t} \right) - 2 \frac{d}{dx} \left(\frac{1}{x - t} \right),$$

$$\int_{-h}^h \frac{v(t)}{t - x} dt = v(h) \log(x - h) + \text{bounded terms, for } x \rightarrow h, x > h,$$

and equation (D.4), the cleavage stress is given by

$$\lim_{x \rightarrow h^+} \sigma_{yy}^2(x, 0) = - \frac{4\mu_3 v(h)}{\pi t} \log(x - h) + \text{Order}(1). \quad (\text{D.5})$$

Appendix E

Numerical Techniques and Convergence of Results

All the computational work was done in double precision on the NAS AS/XL-60 computer at Clemson University. The computer has a double precision unit of $EPS = 0.222 \times 10^{-15}$ and can represent a maximum of 18 decimal digits. All programs were written in FORTRAN.

Crack within the Layer

The Fredholm Kernel \bar{K}_{11} in equation (57) is an integral over a semi-infinite interval and is estimated by using the NAG [32] FORTRAN library routine called D01BAF. It computes an estimate of the integral using the n-point Gauss-Laguerre formula [25], which is exact for any function of the form

$$f(x) = e^{-bx} \sum_{i=0}^{2n-1} c_i x^i \quad (E.1)$$

This routine is appropriate for exponentially decaying functions and the parameter 'b' is chosen to match the decay rate of the function, $f(x)$.

The stress intensity factor, K_I given by equation (61) is the most significant parameter and is tabulated to 6 significant digits as a function of the number 'N' of the Gauss-Chebyshev quadrature formula used in equation (57). Results are given for material combinations MC I and MC V in Table E-I ($\frac{a}{h} = 0.9$, $\frac{t}{h} = 0.1$). It may be mentioned that the techniques [22] used to evaluate the stress intensity factor in this case are based on treating the singular integral equation as a system of Fredholm equations and then finding the unknown function at discrete collocation points.

Table E-I. Stress intensity factor as a function of number of quadrature points (N).

N	Normalized Stress Intensity Factor, $K_I/p_1 \sqrt{a}$	
	Material Combination	
	MC I	MC V
25	2.05261	0.847155
29	2.05262	0.847154
33	2.05262	0.847154
37	2.05262	0.847154
41	2.05262	0.847154

Convergence of the above results needs no explanation. Forty-one quadrature points were used for all combinations.

Crack Up to the Interface

The kernel K_{11} in equation (106) is solved by the techniques explained in the previous section. The finite integral in equation (106) given by

$$I = \int_{-1}^1 h^2 P_n(s) K_{11}(hs, hr_i) ds \quad (E.2)$$

is solved by using the n-point Gauss-Legendre formula [25] exact for any function of the form

$$f(x) = \sum_{i=0}^{2n+1} c_i x^i. \quad (E.3)$$

The formula is appropriate for functions which can be approximated by

polynomials, and is given by

$$\int_a^b f(x) dx = \frac{b-a}{2} \sum_{i=1}^m w_i f(y_i), \quad (\text{E.4})$$

where

$$y_i = \left(\frac{b-a}{2}\right) x_i + \left(\frac{b+a}{2}\right),$$

$$x_i = i^{\text{th}} \text{ zero of } P_m(x),$$

$$w_i = \frac{2}{(1-x_i)^2} [P'_m(x_i)]^2, \quad (\text{E.5})$$

and $P_m(x)$ is a Legendre polynomial.

The stress intensity factor, \tilde{K} is the slowest converging parameter in the problem and is tabulated in Table E-II as a function of the number of collocation points, N for material combinations MC I and MC II ($\frac{t}{h} = 0.2$).

Table E-II. Modified stress intensity factor as a function of number of collocation points (N).

N	Normalized Modified Stress Intensity Factor, \tilde{K}/p_1	
	Material Combination	
	MC I	MC II
24	0.69068	0.79443
28	0.68820	0.79321
32	0.68650	0.79238
36	0.68528	0.79178
40	0.68437	0.79132

Analytically more accurate results can be obtained by increasing the number of collocation points, N . This is limited only by computer time, but for practical purposes and within reasonable accuracy, a limiting value of N is required.

One can estimate the value of the normalized stress intensity factor, \tilde{K}/p_1 , as $N \rightarrow \infty$ by using extrapolation techniques [22,33] for accelerating the convergence of a monotonic sequence (oscillating sequences require modification). The normalized stress intensity factor, \tilde{K}/p_1 , is expressed as a function of the number of quadrature points, N as

$$K(N) = K(\infty) + \frac{B}{N^\alpha}, \quad (\text{E.6})$$

where $K(\infty)$ = estimated value of \tilde{K}/p_1 ,

B = unknown constant,

α = exponential constant.

The three unknowns can be evaluated by using three values of N (N_i , $i = 1, 2, 3$). To ensure stability of the calculated results, the exponential constant, α should be greater than one. Some tabulated values up to four significant digits are given in Table E-III for material combination MC I ($\frac{t}{h} = 0.2$).

Table E-III. Estimated values of the normalized modified stress intensity factor.

N_i	$K(\infty)$	B	α
24,28,32	0.6795	1.985	1.630
28,32,36	0.6796	2.135	1.656
32,36,40	0.6796	2.043	1.641

For material combinations MC I - MC IV, the difference between the estimated value, $K(\infty)$ and the calculated value, $K(40)$ for forty collocation points is less than one percent. Hence forty collocation points are used for all the solutions. For the material combination V, convergence is slower and requires more than forty collocation points to achieve the same accuracy. This difficulty can only be overcome at the expense of computer time.

H-Shaped Crack

The kernel K_{11} and the finite integral in equation (162) are solved by using the techniques explained in the previous sections. The kernel K_{12} given by equation (162) is evaluated by the following procedure for speed and accuracy. The kernel K_{12} can be written as

$$K_{12}(x, z) = K_{12}^{\infty}(x, z) + K_{12}^L(x, z) + K_{12}^F(x, z), \quad (\text{E.7})$$

where

$$K_{12}^{\infty}(x, z) = \int_0^{\infty} k_{12}^{\infty}(x, \eta) \text{Cos } \eta z \, d\eta, \quad (\text{E.8a})$$

$$K_{12}^L(x, z) = \int_0^{\infty} k_{12}^L(x, \eta) \text{Cos } \eta z \, d\eta, \quad (\text{E.8b})$$

$$K_{12}^F(x, z) = \int_0^{\infty} [k_{12}(x, \eta) - k_{12}^{\infty}(x, \eta) - k_{12}^L(x, \eta)] \text{Cos } \eta z \, d\eta. \quad (\text{E.8c})$$

and k_{12}^{∞} is the asymptotic value of the integrand $k_{12}(x, \eta)$ as $\eta \rightarrow \infty$ and $x \rightarrow \pm h$ and is given by

$$k_{12}^{\infty}(x, \eta) = [(d_1 \eta + d_2) \text{Cosh } \eta x + (d_3 \eta + d_4) \text{Sinh } \eta x] e^{-\eta h}, \quad (\text{E.9})$$

and $k_{12}^L(x, \eta)$ includes the terms of order $(1/\eta)$ as $\eta \rightarrow \infty$ and $x \rightarrow zh$, and is given by

$$k_{12}^L(x, \eta) = \left[\frac{d_5}{\eta + d_6} + \frac{d_7}{\eta + d_8} \right] \text{Cosh } \eta x e^{-\eta h} + \left[\frac{d_9}{\eta + d_6} + \frac{d_{10}}{\eta + d_8} \right] \text{Sinh } \eta x e^{-\eta h}, \quad (\text{E.10})$$

where d_i , ($i = 1, \dots, 10$), are explicit expressions in terms of material properties and geometrical parameters.

K_{12}^∞ can be evaluated exactly by using the following exact result [27],

$$\frac{d^m}{dx^m} \int_0^\infty e^{-\eta x} \text{Cos } \eta z \, d\eta = \frac{d^m}{dx^m} \left[\frac{x}{x^2 + z^2} \right], \quad x > 0. \quad (\text{E.11})$$

K_{12}^L is an integral of a slowly converging function $[O(\frac{1}{\eta})]$ over a semi-infinite interval. The following results express the integral K_{12}^L as finite interval integrals and a highly convergent semi-infinite integral.

$$\int_0^\infty \frac{e^{-ax}}{x+b} \text{Cos } cx \, dx = e^{ab} \text{Sin } (bc) \left[\text{Tan}^{-1} \frac{c}{a} - \int_0^b \frac{e^{-ax} \text{Sin } cx}{x} \, dx \right] + e^{ab} \text{Cos } (bc) \left[-\frac{1}{2} \log \left(\frac{c^2 + a^2}{a^2} \right) + \int_0^b \frac{1 - \text{Cos } cx}{x} e^{-ax} \, dx + E_1(ab) \right], \quad (\text{E.12})$$

$a > 0, b > 0$

where $E_1(x)$ is the exponential integral defined by

$$E_1(x) = \int_x^\infty \frac{e^{-u}}{u} \, du, \quad x > 0. \quad (\text{E.13})$$

The finite integrals in equation (E.12) are estimated by using a NAG [32] library routine D01AKF, an adaptive integrator suitable for oscillating integrands. It uses Gauss 30-point and Kronrod 61-point rules. Another NAG [32] library routine S13AAF calculates an approximate value of the exponential integral $E_1(x)$.

The break-up of the integral as given by equation (E.7) allows the kernel K_{12} to be evaluated accurately and rapidly because the integrand of K_{12}^F decays at least at the rate of $e^{-\eta h}$, where 'h' is the half layer width. K_{12}^F is evaluated by using a NAG [32] library routine D01ANF, an adaptive integrator for finite cosine or sine transforms. In view of the fast convergence [$O(e^{-\eta h})$] of the integral and definition of K_{12}^F , the upper limit in the integral can be substituted as $200/h$.

The rest of the kernels in equations (162-164) are evaluated similarly by breaking up the integrand in form of equation (E.7) and using the following additional results.

$$\frac{d^m}{dx^m} \int_0^{\infty} e^{-\eta x} \sin \eta z \, d\eta = \frac{d^m}{dx^m} \left(\frac{z}{x^2 + z^2} \right), \quad x > 0, \quad (\text{E.14})$$

$$\begin{aligned} \int_0^{\infty} \frac{e^{-ax}}{x+b} \sin cx \, dx &= e^{ab} \cos(bc) \left[\tan^{-1} \frac{c}{a} - \int_0^b \frac{e^{-ax} \sin cx}{x} \, dx \right] \\ &\quad - e^{ab} \sin(bc) \left[-\frac{1}{2} \log \left(\frac{c^2 + a^2}{a^2} \right) \right. \\ &\quad \left. + \int_0^b \frac{1 - \cos cx}{x} e^{-ax} \, dx + E_1(ab) \right], \\ &\quad a > 0, \quad b > 0, \quad (\text{E.15}) \end{aligned}$$

$$\begin{aligned} \int_0^{\infty} \frac{\cos ax}{x+b} \, dx &= -\sin(ab) \left[\text{Si}(ab) - \frac{\pi}{2} \right] \\ &\quad - \cos(ab) \text{Ci}(ab), \quad a > 0, \quad b > 0, \quad (\text{E.16}) \end{aligned}$$

$$\int_0^{\infty} \frac{\sin ax}{x+b} dx = \sin(ab) \text{Ci}(ab) - \cos(ab) \left[\text{Si}(ab) - \frac{\pi}{2} \right], \quad a > 0, b > 0. \quad (\text{E.17})$$

The NAG [32] library routines S13ACF and S13ADF estimate the value of the cosine integral $\text{Ci}(x)$ and the sine integral $\text{Si}(x)$, respectively which are defined [25] as

$$\text{Ci}(x) = \gamma + \log x + \int_0^x \frac{\cos t - 1}{t} dt, \quad x > 0, \quad (\text{E.18})$$

$$\text{Si}(x) = \int_0^x \frac{\sin t}{t} dt, \quad x > 0, \quad (\text{E.19})$$

where γ = Euler's constant (= 0.577215 ...).

Equations (E.12) and (E.15) may give erroneous results for $|ab| > 5$ due to round-off errors. For such cases, the integral is directly solved by using the NAG [32] library routine, D01ANF, an adaptive integrator for cosine or sine transforms of a function over a finite interval. The upper limit in the integral is taken as $200/b$, where b is the exponential decay rate of the integrand K_{12} .

All the finite integrals in equations (162-164) are solved by using the technique explained in the second section of this appendix.

To illustrate the convergence of the results, the normalized stress intensity factor, \hat{K}/p_1 is tabulated as a function of the collocation points of the quadrature scheme used in equations (162-164) for material combinations MC I ($\frac{c}{h} = 0.05$, $\frac{t}{h} = 0.2$) and MC II ($\frac{c}{h} = 0.002$, $\frac{t}{h} = 0.2$).

Table E-IV. Modified stress intensity factor as a function of number of collocation points (K, L, M).

K=L=M	Normalized Modified Stress Intensity Factor, $\frac{\Delta}{K/p_1}$	
	Material Combination	
	MC I	MC II
24	0.36473	0.39367
28	0.36461	0.39320
32	0.36454	0.39296
36	0.36450	0.39287
40	0.36447	0.39287

Applying the same extrapolation technique and accuracy criterion illustrated in the previous section, forty collocation points (K=L=M=40) are found to be sufficient for material combinations MC I - MC IV. For the material combination MC V, the convergence is slower and requires more than forty collocation points. This difficulty can be overcome at the expense of computer time.

Appendix F
Letter of Consent



American Cyanamid Company
Stamford Research Laboratories
1937 West Main Street
P.O. Box 60
Stamford, Conn. 06904 - 0060
Tel. (203) 348-7331

June 18, 1987

Mr. Autar K. Kaw
Department of Mechanical Engineering
318 Riggs Hall
Clemson University
Clemson, South Carolina 29634-0921

Dear Mr. Kaw:

Please excuse my tardiness in issuing this formal, written response to your request for photographs. As I indicated during our telephone conversation, including these photographs (i.e. Figs. 2, 13 and 14 from my paper entitled "Characterization of Impact Damage in Graphite/Epoxy Laminates") in your report presents no problem. I hope this letter will meet your requirements for a formal consenting letter. If not, please call and I will be happy to respond.

As we also discussed during our telephone conversation, I would be most interested in receiving a copy of your final report.

Sincerely yours,


John E. Masters

JEM:saj
Doc. (1.20)

LIST OF REFERENCES

1. Masters, J.E., "Characterization of Impact Damage Development in Graphite/Epoxy Laminates," ASTM Symposium on Fractography of Modern Engineering Materials, Nashville, TN, November 1985.
2. Sun, C.T., "Suppression of Delamination in Composite Laminates Subjected to Impact Loading," 11th Annual Mechanics of Composite Review, Dayton, OH, pp. 106-113, October 1985.
3. Sneddon, I.N. and Srivastav, R.P., "The Stress Field in the Vicinity of a Griffith Crack in a Strip of Finite Width," International Journal of Engineering Sciences, Vol. 9, pp. 479-488, 1971.
4. Gupta, G.D. and Erdogan, F., "The Problem of Edge Cracks in an Infinite Strip," ASME Journal of Applied Mechanics, Vol. 41, pp. 1001-1006, December 1974.
5. Hilton, P.D. and Sih, G.C., "A Laminate Composite with a Crack Normal to the Interfaces," International Journal of Solids and Structures, Vol. 7, pp. 913-930, 1971.
6. Bogy, D.B., "The Plane Elastostatic Solution for a Symmetrically Loaded Crack in a Strip Composite," International Journal of Engineering Science, Vol. 11, pp. 985-996, 1973.
7. Ashbaugh, N.E., "Stresses in Laminated Composites Containing a Broken Layer," ASME Journal of Applied Mechanics, Vol. 40, pp. 533-540, June 1973.
8. Gupta, G.D., "A Layered Composite with a Broken Laminate," International Journal of Solids and Structures, Vol. 9, pp. 1141-1154, 1973.
9. Erdogan, F. and Bakioglu, M., "Stress-Free End Problem in Layered Materials," International Journal of Fracture, Vol. 13, pp. 739-749, 1977.
10. Gecit, M.R. and Erdogan, F., "The Effect of Adhesive Layers on the Fracture of Laminated Structures," ASME Journal of Engineering Materials and Technology, Vol. 100, pp. 2-9, 1978.
11. Cook, T.S. and Erdogan, F., "Stresses in Bonded Materials with a Crack Perpendicular to the Interface," International Journal of Engineering Science, Vol. 10, pp. 677-697, 1972.

12. Goree, J.G. and Venezia, W.A., "Bonded Elastic Half-Planes with an Interface Crack and Perpendicular Intersecting Crack That Extends into the Adjacent Material," International Journal of Engineering Science, Vol. 15, Part 1, pp. 1-17; Part 2, pp. 19-27, 1977.
13. Lu, M. and Erdogan, F., "Stress Intensity Factors in Two Bonded Elastic Layers Containing Cracks Perpendicular to and on the Interface," Engineering Fracture Mechanics, Vol. 18, Part 1, pp. 491-506; Part 2, pp. 507-528, 1983.
14. Comninou, M., "The Interface Crack," ASME Journal of Applied Mechanics, Vol. 44, pp. 631-636, December 1977.
15. Gautesen, A.K. and Dundurs, J., "The Interface Crack in a Tension Field," ASME Journal of Applied Mechanics, Vol. 54, pp. 93-98, March 1987.
16. Knowles, J.K. and Sternberg, E., "Large Deformations Near a Tip of an Interface Crack Between Two Neo-Hookean Sheets," Journal of Elasticity, Vol. 13, pp. 257-293, 1983.
17. Hadamard, J., "Lectures on Cauchy's Problems in Linear Partial Differential Equations," Yale University Press, 1923.
18. Erdogan, F., Gupta, G.D. and Cook, T.S., "On the Numerical Solution of Singular Integral Equations," Method of Analysis and Solution to Crack Problems, Edited by G.C. Sih, Noordhoff, 1972.
19. Timoshenko, S.P. and Goodier, J.N., "Theory of Elasticity," McGraw Hill, 1970.
20. Muskhelishvili, N.I., "Singular Integral Equations," Noordhoff, 1953.
21. Krenk, S., "A Note on the Use of the Interpolation Polynomial for Solutions of Singular Integral Equations," Technical Report, Lehigh University, August 1973.
22. Erdogan, F. and Gupta, G.D., "On the Numerical Solution of Singular Integral Equations," Quarterly Journal of Applied Mathematics, pp. 525-534, January 1972.
23. Erdelyi, A., "Tables of Integral Transforms," Vol. 1, New York, McGraw Hill, 1953.
24. Bogy, D.B., "On the Problem of Edge-Bonded Elastic Quarter Planes Loaded at the Boundary," International Journal of Solids and Structures, Vol. 6, pp. 1287-1313, 1970.
25. Abramowitz, M. and Stegun, I.A., "Handbook of Mathematical Functions," National Bureau of Standards, Applied Mathematics Series 55, 1964.

26. Kaya, A.C. and Erdogan, F., "On the Solution of Integral Equations with Strong Singularities," Proceedings of an IMACS International Symposium, Lehigh University, Pennsylvania, pp. 54-57, 1984.
27. Tricomi, F.G., "Integral Equations," Interscience, New York, 1957.
28. Fox, L. and Parker, I.B., "Chebyshev Polynomials in Numerical Analysis," London, Oxford U.P., 1968.
29. Wolla, J.M. and Goree, J.G., "Experimental Evaluation of Longitudinal Splitting in Unidirectional Composites," Journal of Composite Materials, Vol. 21, pp. 49-67, 1987.
30. Erdogan, F., "Simultaneous Dual Integral Equations with Trigonometric and Bessel Kernels," Zeitschrift Fur Angewandte Mathematik und Mechanik (ZAMM), Band 48, Heft 4, pp. 217-225, 1968.
31. Dundurs, J., "Effect of Elastic Constants on Stress in a Composite Under Plane Deformations," Journal of Composite Materials, Vol. 1, pp. 310-322, 1967.
32. NAG FORTRAN Library Manual, Vol. 1-6, Numerical Algorithms Group, December 1982.
33. Davis, P.J. and Rabinowitz, P., "Numerical Integration," Blaisdell Publishing Company, 1967.